14

From Laminar Flow to Turbulence

Geoffrey K. Vallis

14.1 Preamble and Basic Ideas

Fluid dynamics in general, and turbulence in particular, is a most nonlinear field. The subjects are enormous; one need only browse through Monin and Yaglom [1] to see this. This chapter is not a review of turbulence, for in a few pages any attempt at an overview would certainly be ambitious and perhaps even foolish; rather, it is didactic introduction into just a couple of aspects, one of fairly recent origin and one with more traditional roots. We will first describe various routes involved in the *transition* to turbulence. This is a subject that has undergone a revolution in the past 20 or 30 years. It has greatly affected how we think about, although not how we calculate the properties of, our second topic of discussion, namely *fully developed*, or (especially in the Russian literature) *strong* turbulence. In fact, statistical theories of strong turbulence seem to be oblivious (perhaps with good reason) to theories and routes regarding transition. In both areas our discussion is rather selective, concentrating on the utility of scaling arguments and self-similarity. These properties allow the application of renormalization arguments in simple maps (e.g., the logistic map), enabling quantitative predictions to be made regarding the onset of chaos; remarkably, some of these have been verified in some real fluid dynamical experiments. Scaling arguments also lie at the heart of phenomenological theories of strong turbulence of the "Kolmogorov type," for which there is also observational support. We give rather short shrift to descriptions of experimental evidence and observations, simply referring the reader to the original literature, not because the area is not important but because it deserves much more space than we can give it here. In other ways, too, our discussion is incomplete, for nowhere do we discuss certain well-known prototypical problems such as the Lorenz equations, partly because such discussions abound elsewhere.

In turbulence, nonlinear interactions connect motions on different scales, leading to unpredictability on all scales of flow even when the error in the initial conditions is confined to small scales. This provides motivation (if any were needed) for our travails by way of a very practical question, for how long can we forecast the weather? The rapid loss of information in the smaller

scales of motion suggests that one should attempt to treat the smaller scales *parametrically* in terms of the better-resolved and better-predicted large scales, and we will briefly discuss current approaches to this problem (the eddy diffusivity problem). Again, self-similarity and scaling allows the use of renormalization-type methods, in particular successive averaging methods, to rescale the diffusivity and obtain a parameterization of small scale motions. Space will forbid us exploring many of the side issues of these problems. Although the presentation is a little less abstract, and more overtly fluid dynamical than that often found in expositions to do with the onset of chaos, we do not approach the range of fluid dynamical problems discussed in various fluid dynamical texts (e.g. [2]). We have drawn on discussions by Hu and by Landau and Lifshitz [3] as well as original sources cited in the text. The reviews of Miles and of Eckmann, which cover similar ground in rather different styles, and of Rose and Sulem, are also recommended reading [4].

The equations describing fluid motion (14.1) are manifestly and nontrivially nonlinear, and historically much of the "early" (i.e., circa 1960–1975) development of nonlinear dynamics was in fact motivated by problems in fluid dynamics. Many of the applications of the modern theory of nonlinear dynamics (often loosely called "chaos theory") have been applied, with some success, to the theory of the it transition to turbulence (or more accurately the transition to chaos) where a few degrees of freedom might be expected to dominate the flow. A successful theory of strong turbulence has, on the other hand, proved very elusive, although the statistical approaches based on renormalized perturbation theories (beginning with the Direct Interaction Approximation [5]) have contributed a great deal. There is still much controversy about whether deterministic, "dynamical systems" approaches to turbulence are even appropriate, because of the relatively high dimensionality of fully turbulent flow. Furthermore, the parameter space over which low-dimensional, transitional behavior occurs is rather small compared to that over which fully turbulent behavior occurs. Thus, weak turbulence is the exception, rather than the rule, and the natural philosopher is led to ponder why she should study it at all. One answer, superficially trite, is that it is a field where true progress can and has been made; the investigator's hope, springing eternal, is that further investigation along the same lines may lead to substantial attacks on the theory of strong turbulence. In this chapter we first discuss the theory of transition, and then direct attention toward *statistical* attacks (based on Kolmogorovian phenomenology) into just a couple of aspects of strong turbulence: namely, the predictability problem and the eddy diffusivity problem.

14.1.1 What Is Turbulence?

The equations describing constant density flow phenomena are the Navier–Stokes equations; namely:

$$\frac{\partial \mathbf{u}}{\partial t} + (\mathbf{u} \cdot \nabla)\mathbf{u} = -\frac{1}{\rho}\nabla p + \nu \nabla^2 \mathbf{u} \tag{14.1}$$

along with the mass continuity constraint

$$\nabla \cdot \mathbf{u} = 0. \tag{14.2}$$

Here, $\mathbf{u}(x, y, z, t)$ is the velocity field, p is the pressure, ρ the density (henceforth taken as unity), and ν the kinematic viscosity. These equations, with appropriate boundary conditions, determine the evolution of most incompressible fluid phenomena.

If U is a typical velocity magnitude, and L a typical length scale, then the Reynolds number, $Re = UL/\nu$ is a useful nondimensional measure of the ratio of the inertial terms to the viscous terms. Laminar flow may be defined as that flow for which the field variables $(\mathbf{u}, p)$ are time independent, or vary in a periodic way. In some particular flow geometry or experimental configuration, we may imagine being able to control the Reynolds number externally, perhaps by increasing the pressure difference along a pipe, or increasing the shear in a parallel flow as we discuss in section 14.2. As this is done, one typically finds that at some critical value the time-independent flow becomes unstable, and the flow bifurcates into some other configuration, perhaps a periodically varying flow. As Reynolds number increases further bifurcations occur, their precise nature and sequence depending on the flow at hand. After a small number of bifurcations the flow is frequently completely chaotic. Now, chaos is often taken as meaning the superficially random temporal behavior of a possibly small number of variables, as seen for example in the Lorenz equations or any number of well-known systems. A positive Lyapunov exponent is a common indicator of chaos. Fluid turbulence, in its usual sense, is also taken to imply *spatiotemporal* chaos, implicitly involving a larger number of degrees of freedom. That is, although strong turbulence almost certainly implies chaos, it is much more than that. Still, the distinction is sometimes *overemphasized*, because even fully developed turbulence has to all intents and purposes, a finite number of excited degrees of freedom and can be described as accurately as we wish by a system (albeit large) of ordinary differential equations. In any case, although the transition from "chaos" to "turbulence" in a fluid is not quantitatively understood, once chaos has arisen turbulence is thought to follow very shortly, or even immediately, thereafter. Because of the large number of degrees of freedom it then becomes sensible to seek a statistical approach in which a completely deterministic description of the fluid is foregone in favor of a description of averages. The reasons are twofold. First, a large number of degrees of freedom makes determinism extremely clumsy. Second, even if we could follow every eddy, the unpredictability of the fluid motion would make such knowledge useless, because the initial conditions of small scales of motion are not given. Thus,

unless we were to perform Monte Carlo simulations with a range of initial conditions for the unobserved small scales, a statistical picture (or a description of mean quantities using some parameterization, or closure) is actually demanded. However, because of the nonlinearity of the equations this is very difficult; starting with any nonlinear equations of the from

$$\frac{da}{dt} = aa, \tag{14.3}$$

the equation for a mean quantity $\bar{a}$ is of the from

$$\frac{d\bar{a}}{dt} = \bar{a}\bar{a} + \overline{a'a'}, \tag{14.4}$$

where a prime denotes a deviation from the mean. The equation for $\overline{a'a'}$ involves triple correlations, those for triple correlations fourth order terms, and so on in an unclosed heirarchy. Earlier approaches to turbulence, such as the Direct Interaction Approximation [5], concentrated on "closing" this heirarchy, by the introduction of assumptions not directly deducible from the equations of motion, but without using the scaling properties of the Navier–Stokes equations described in Section 14.4. This turned out to be a very difficult road to follow, and in fact may be demanding too much. More recent approaches have *started* with the scaling properties, and built from there. Whichever, if either, approach turns out to reveal more, it is fair to say that a completely satisfactory statistical description of turbulence at this time does not exist.

14.2 From Laminar Flow to Nonlinear Equilibration

The Navier–Stokes equations are tremendously verdent, and depending on the boundary conditions or the nature of the fluid a myriad of flows are possible, each being controlled by various nondimensional parameters. For adiabatic, incompressible flow (as, for example, in water flow in a pipe) the Reynolds number is the controlling parameter in a given geometry. In problems in convection (usually fluid in a constant gravitational field heated from below, or cooled from above) a relevant control parameter is the Rayleigh number, $g\alpha\Delta T d^3/(\nu\kappa)$, where g is gravity, α measures the thermal expansion, d is a length scale, ΔT a typical temperature difference, and ν and κ are inertial and thermal diffusivities, respectively. In rotating fluids the Ekman number, $\nu/(2\Omega L^2)$, where Ω is the rate of rotation, and the Rossby number, $U/(2\Omega L)$, determine the relative importance of friction and rotation. In different geometries other parameters may play a role. Given this rich structure, it would be very surprising if there were only one "route to chaos" in fluids,

and indeed there is not. However, it does seem that there may be a small number (perhaps in single digits) of recognizably different transition scenarios. By scenario we mean a qualitatively distinct path (sequence) with certain characteristic behavior; we do not mean necessarily identical behavior in each case. Now, each sequence often begins with a *linear instability*, in which a steady (i.e., time independent) flow satisfying the Navier–Stokes equations becomes unstable. Before plunging into nonlinear analysis, let us analyze a simple linear instability.

14.2.1 A Linear Analysis: The Kelvin–Helmholtz Instability

The simplest instance of a linear instability, which is also of some physical interest, is perhaps the Kelvin–Helmholtz instability. This is a shear instability, in which two fluids sliding against one another, or one fluid with a strong shear perpendicular to its mean velocity, become unstable. We will consider the simplest case, that of two fluids of equal density, with a common surface at $z = 0$, moving with velocities $-U$ and $+U$ in the x-direction, respectively (Fig. 14.1). There is no variation in the basic flow in the y-direction, and we will assume this is also true for the instability. This flow is clearly a solution of the inviscid Navier–Stokes equations (the Euler equations). The question to be asked is, what happens if the flow is perturbed slightly? We will neglect variations in the y-direction (these are unnessential to the instability) and, for the moment, also neglect friction. If the perturbation is initially small, then even if it grows we can, for small times after the onset of instability, neglect the nonlinear interactions in the governing equations because these are the squares of small quantities. The equations determining the evolution of the initial perturbation are then the Navier–Stoke equations (14.1), linearized about the steady solution. Thus, for $z > 0$

$$\frac{\partial \mathbf{u}'}{\partial t} + U\frac{\partial \mathbf{u}'}{\partial x} = -\nabla p', \tag{14.5a}$$

$$\nabla \cdot \mathbf{u}' = 0, \tag{14.5b}$$

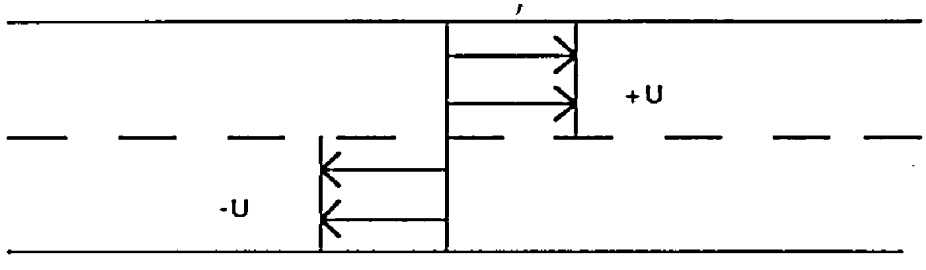

FIGURE 14.1. Basic flow giving rise to Kelvin–Helmholtz instability. For the problem as solved in the text, the boundaries are removed to infinity.

with a similar equation but with U replaced by $-U$ for $z < 0$. (The density is unity, so does not appear.)

We can represent the perturbations by a Fourier expansion of the from

$$\phi(x, z, t) = \sum_k \hat{\phi}_k(z, t) \exp[ikx], \tag{14.6}$$

where ϕ is any field variable (pressure or velocity). Because (14.5) is linear, the Fourier modes do not interact and we confine attention to just one. Taking the divergence of Eq. (14.5a), the left-hand side vanishes and the pressure satisfies Laplaces equation

$$\nabla^2 p' = 0. \tag{14.7}$$

For $z > 0$, this has solutions in the form

$$p' = \hat{p}_1 e^{ikx+\theta t} e^{-kz}, \tag{14.8}$$

where we have also introduced the explicit time dependence $e^{\theta t}$. In general θ is complex; if the soon-to-be-found dispersion relationship gives θ with a positive real component, we have an instability. Any imaginary component gives oscillatory motion. To obtain the dispersion relationship, we consider the z-component of (14.5), namely (for $z > 0$)

$$\frac{\partial w_1'}{\partial t} + U\frac{\partial w_1'}{\partial x} = -\frac{\partial p_1'}{\partial z}. \tag{14.9}$$

Substituting a solution of the form $w_1' = \hat{w}_1 \exp(ikx + \theta t)$ yields, with Eq. (14.8),

$$(\theta + ikU)\hat{w}_1 = k\hat{p}_1. \tag{14.10}$$

But the velocity normal to the discontinuity is, at the discontinuity, nothing but the rate of change of the discontinuity itself. That is, at the interface $z = +0$

$$w_1 = \frac{\partial \zeta}{\partial t} + U\frac{\partial \zeta}{\partial x}, \tag{14.11}$$

or

$$(\theta + ikU)\hat{\zeta} = \hat{w}_1. \tag{14.12}$$

Using this in Eq. (14.10) gives

$$(\theta + ikU)^2\hat{\zeta} = k\hat{p}_1. \tag{14.13}$$

The above few equations pertain to motion on the $z > 0$ side of the interface. Similar reasoning on the other side gives (at $z = -0$)

$$(\theta - ikU)^2\hat{\zeta} = -k\hat{p}_2. \tag{14.14}$$

But, at the interface $p_1 = p_2$ (because pressure must be continuous). The dispersion relationship then emerges from Eq. (14.13) and (14.14), giving

$$0^2 = k^2 U^2. \tag{14.15}$$

Thus the flow is *unstable* and the amplitude of any small perturbation will initially grow exponentially. The instability itself can be seen in the natural world when billow clouds appear wrapped up into spirals: the clouds are acting as tracers of fluid flow, indicating a shear in the atmosphere. The interested reader should peruse Ludlum's wonderful book *Clouds and Storms* [6].

In our ideal example the instability appears immediately; that is, no matter how small the shear. The reason for this is the neglect of viscosity, so that the Reynolds number is always infinite. If viscosity is retained, the analysis becomes a little more involved, in part because the basic state cannot have a velocity discontinuity. Most approaches involve allowing the velocity shear to vary smoothly. The instability now sets in only when the shear is sufficiently large; that is, when an appropriate Reynolds number reaches some critical value. Suppose that the initial value of the shear *is* slightly supercritical. Then the linear analysis tells us a perturbation will grow exponentially. But of course a real instability (if only on energetic grounds) cannot keep growing. In fact the perturbation will eventually reach finite amplitude, at which point a nonlinear analysis is necessary.

14.2.2 A Weakly Nonlinear Analysis: Landau's Equation

In this section our approach starts to get more abstract, and we deviate from a strict analysis of the governing equations. To discuss this it is helpful to know what a Hopf bifurcation is (Figs. 14.2 and 14.3). (For more detailed descriptions of bifurcations in hydrodynamics, see for example the article by Joseph in Swinney and Gollub [2].) Suppose that the linearization of a system (about a solution) has complex eigenvalues $\{\sigma_i\}$, such that the evolution of the system is proportional to $\exp[\sigma_i t]$, whose values depend on some parameter of the system, say R (e.g., the Rayleigh or Reynolds numbers in fluid dynamics). For $R < R_c$, where R_c is some critical value, suppose the eigenvalues lie in the left half of the complex plane. Then if the system is perturbed, it will damp back to equilibrium in an oscillatory fashion. If at $R = R_c$ one complex conjugate pair crosses the imaginary axis, then the system becomes unstable, and an oscillatory growth takes place on perturbation. A Hopf bifurcation has occurred. (Engineers sometimes call the ensuing kind of instability an overstability). Landau was among the first people to consider how a fluid might equilibrate after such a bifurcation; his argument may be paraphrased as follows. For values of R close to R_c and for small times after the onset of instability, the amplitude of the flow may be expected to behave something like

$$A(t) = C(t)e^{\theta t}, \tag{14.16}$$

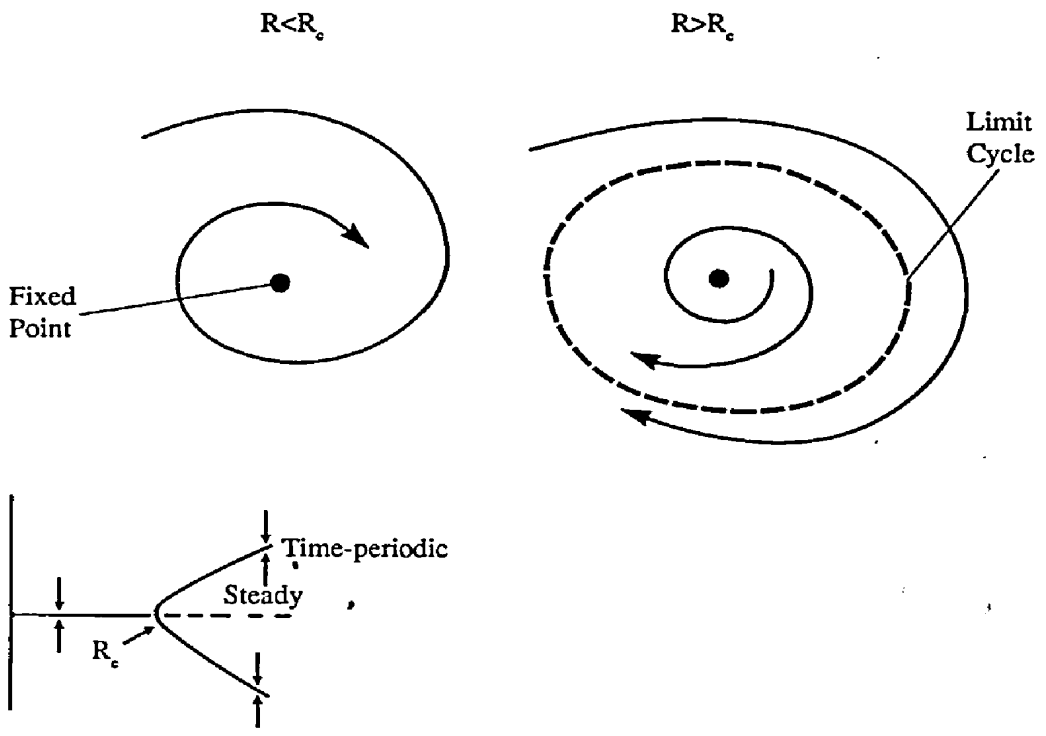

FIGURE 14.2. The supercritical Hopf bifurcation. (A positive Landau constant.) After the bifurcation at R_c the flow converges to a stable limit cycle.

where A is a measure of the amplitude of some field variable (it might, for example, be a Galerkin component). A is in general complex; implicit as usual is the addition of a complex conjugate to ultimately obtain a real field. θ is also complex and may be written $\theta = \sigma + i\omega$. We expect that $\sigma = f(R - R_c)$ and that for $R < R_c$, $\sigma < 0$. That is, the flow is stable and a small perturbation would be damped to zero. The parameter $C(t)$ will, for small times, be a constant, and the amplitude will exponentially grow. The differential equation satisfied by (14.16) is then

$$\frac{d|A|^2}{dt} = 2\sigma|A|^2. \tag{14.17}$$

For longer times this equation cannot be valid, and higher-order terms must enter. Now, if the flow is just supercritical, the growth rate, σ, can be expected to be small and in particular $\sigma \ll |\omega|$. Thus, the flow undergoes an oscillatory instability (see Fig. 14.4). We are interested in its behavior on the timescale $1/\sigma$, averaged over many oscillations. Adding in higher-order terms to Eq. (14.17)

$$\frac{d|A|^2}{dt} = 2\sigma|A|^2 + a_1|A|^2A + a_2|A|^4 \ldots$$

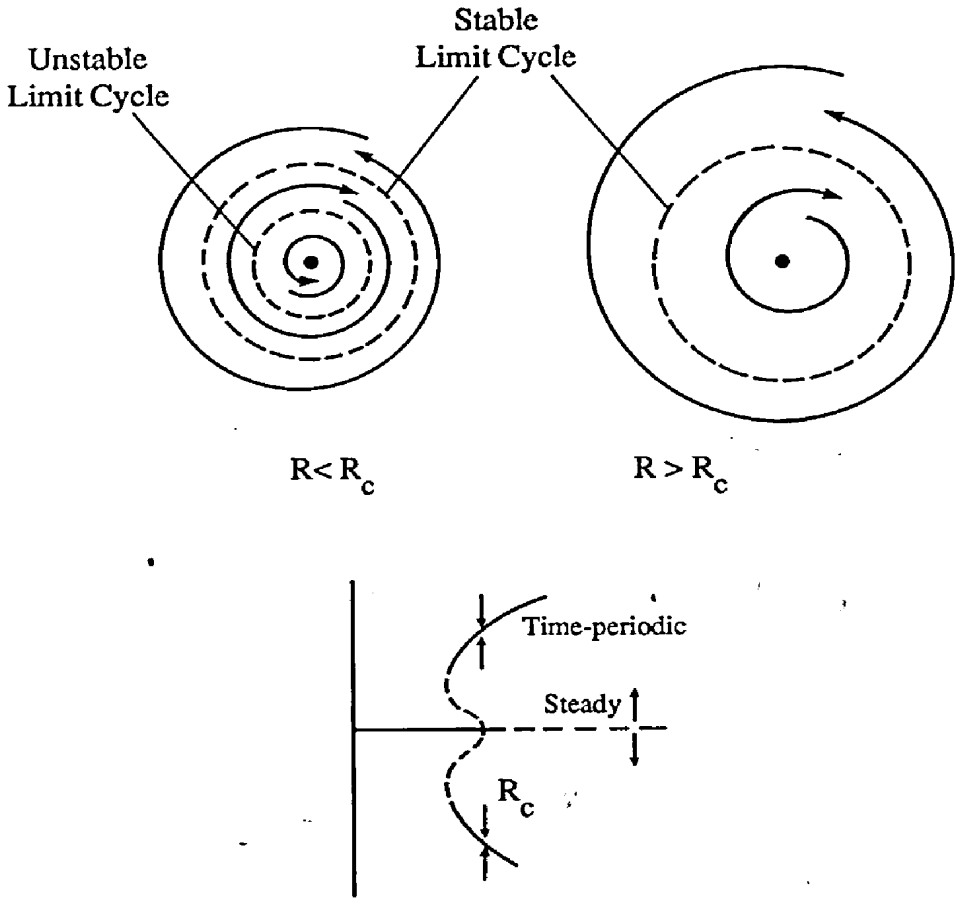

FIGURE 14.3. The subcritical Hopf bifurcation. The outer (stable) limit cycle exists only in the presence of higher-order nonlinearities, absent in our treatment of the Landau equation.

Averaging over the oscillatory time period, the third-order terms will vanish (or actually give a fourth-order contribution) because they contain an oscillatory term. We are left with the fourth-order term, and the Landau equation:

$$\frac{d|A|^2}{dt} = 2\sigma|A|^2 - \alpha|A|^4, \tag{14.18}$$

where α is an undetermined parameter (the Landau constant), which may be positive or negative.

The method of derivation of Eq. (14.18) is really just an application of the method of averaging. The observation that multiple time scales are present (i.e., the slow growth rate and the fast oscillation) suggests one might explicitly employ a multiple time-scale analysis to actually derive the Landau equation, directly from a prototype equation for hydrodynamical and other

instabilities. This we shall now do, although our prototype is rather simple and not explicitly hydrodynamical.

Consider, then, the simple system:

$$\frac{dx}{dt} = \sigma x - \omega y + f_1(x,y) \tag{14.19}$$

$$\frac{dy}{dt} = +\omega x + \sigma y + f_2(x,y). \tag{14.20}$$

The function f_1 and f_2 contain nonlinear terms, and are small and analytic but otherwise arbitrary. These prototype equations therefore contain growth, an oscillation, and nonlinearity, many of the features of a real fluid instability. We shall recognize that growth is slow by writing $\varepsilon = \sigma/\omega \ll 1$. Dividing through by ω, defining a new (nondimensional) time by ωt, and writing $z = x + iy$ we obtain:

$$\frac{dz}{dt} = \varepsilon z + iz + \varepsilon g(z), \tag{14.21}$$

where we now explicitly recognize the smallness of the nonlinear term $\varepsilon g(z)$. There is a similar equation for z^*. The analysis now proceeds by introducing

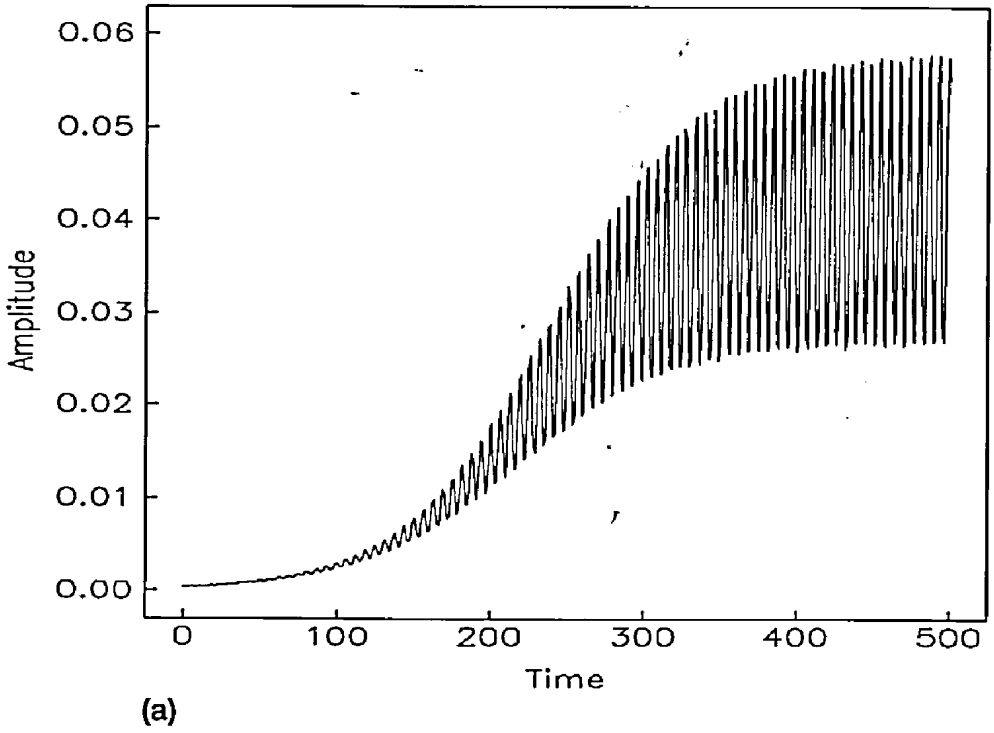

FIGURE 14.4. (a) Amplitude growth obtained by numerically integrating Eqs. (14.19) and (14.20).

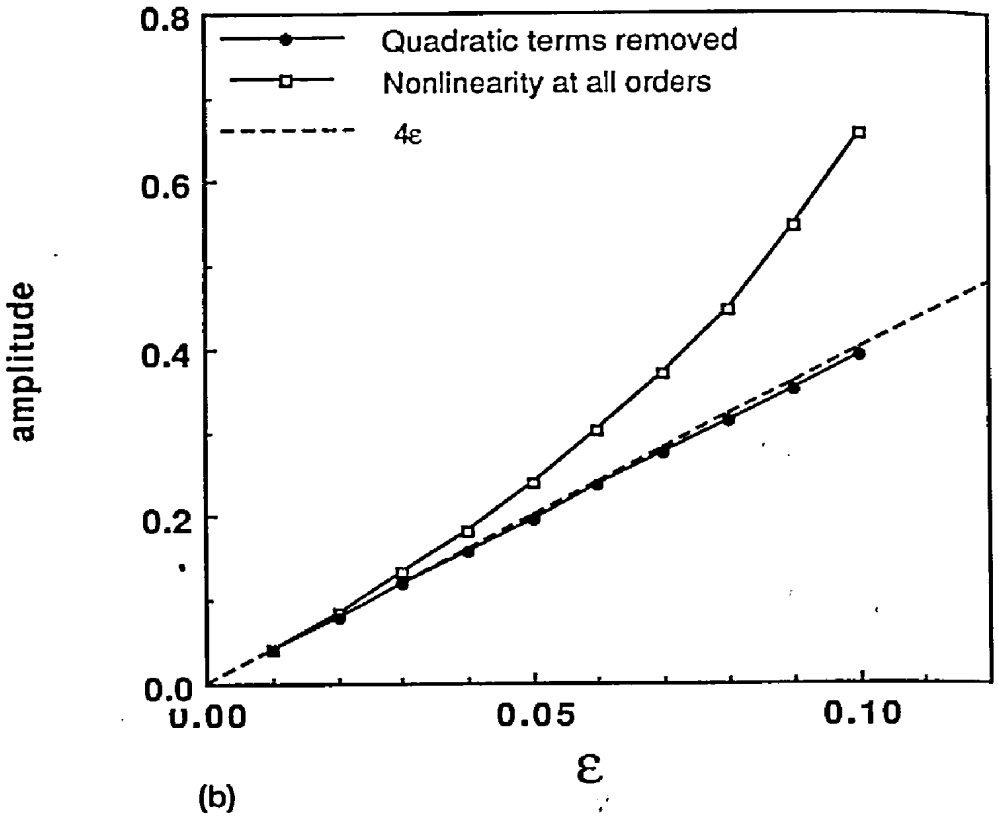

FIGURE 14.4 *(continued)*. (b) Time-averaged equilibrated amplitudes obtained numerically (dots and open squares) compared to prediction from Landau equation (dashed line).

the *slow time* $\tau = \varepsilon t$ and assuming that z is a function of both t and τ. (If the reader is not familiar with this device, it is explained further in a number of books on asymptotic methods; e.g., Bender and Orszag [7].) Thus,

$$\frac{dz}{dt} = \frac{dz}{dt} + \frac{dz}{d\tau}\frac{d\tau}{dt} = \frac{dz}{dt} + \varepsilon\frac{dz}{d\tau}. \tag{14.22}$$

Then we expand z in the series:

$$z(t,\tau) = z_0(t,\tau) + \varepsilon z_1(t,\tau)\ldots \tag{14.23}$$

Using Eq. (14.22) we obtain, to lowest order

$$\frac{dz_0}{dt} = iz_0, \tag{14.24}$$

which has solutions

$$z_0 = C(\tau)e^{it}. \tag{14.25}$$

This of course is just the fast oscillation. To obtain the expression for the slow change in amplitude of z, we go to next order and obtain:

$$\frac{dz_0}{d\tau} + \frac{dz_1}{dt} = z_0 + iz_1 + g(z_0). \tag{14.26}$$

Because z is small, we assume that we may expand the function $g(z_0)$ in powers of z_0, noting that linear terms are already taken care of, whence Eq. (14.26) becomes

$$\frac{dz_1}{dt} - iz_1 = z_0 - \frac{dz_0}{d\tau} + O(z_0^2) + O(z_0^3)\ldots \tag{14.27}$$

or, explicitly in terms of x and y

$$\frac{dx_1}{dt} + y_1 = x_0 - \frac{dx_0}{d\tau} + O(x_0^2, y_0^2) + O(x_0^3, y_0^3)\ldots \tag{14.28a}$$

$$\frac{dy_1}{dt} - x_1 = y_0 - \frac{dy_0}{d\tau} + O(x_0^2, y_0^2) + O(x_0^3, y_0^3)\ldots \tag{14.28b}$$

Now, by assumption εz_1 is smaller than z_0. Thus, for our analysis to be consistent (and consistency, not uniqueness, is all that can reasonably be demanded of an asymptotic analysis) there can be no secular terms (i.e., terms that grow linearly with time) in the form of z_1. Because a solution of the homogeneous equation $dz_1/dt - iz_1 = 0$ is $z \propto e^{it}$, secular terms are eliminated if terms proportional to it vanish on the right-hand side, because secular terms arise when an oscillator is forced at its natural, unperturbed, frequency. The quadratic terms do not contribute to this, but the cubic terms do [this is evidently also seen to be true for Eqs. (14.28a) and (14.28b)], and so secular terms are avoided if

$$\frac{dz_0}{d\tau} = z_0 + a_2|z_0|^2 z_0, \tag{14.29}$$

where a_2 is determined by the projection of the cubic terms proportional to $(\exp[it])^3$ onto $\exp[it]$. Eq. (14.29) leads directly to the Landau equation, and is itself sometimes called a Landau equation.

To be more explicit, consider a particular choice of nonlinear function $f_1(x,y) = f_2(x,y) = \exp(x+y) - (1+(x+y))$. (These arbitrarily chosen functions have nonlinearity at all orders. Any number of other functions would give similar behavior, and there is no necessity to choose $f_1 = f_2$, although it makes the algebra a little easier.) Letting $x(t) = x_0(t,\tau) + \varepsilon x_1(t,\tau)\ldots$, and similarly for y, the *zero*th order balance is:

$$\begin{aligned} \frac{dx_0}{dt} &= -y_0 \\ \frac{dy_0}{dt} &= x_0 \end{aligned} \tag{14.30}$$

with solution $x_0 = X_0(\tau)\cos t, y_0 = Y_0(\tau)\sin t$ [cf. Eq. (14.25)]. At next order Eq. (14.28) is

$$\frac{dx_1}{dt} + y_1 = \left(X_0 - \frac{dX_0}{d\tau}\right)\cos t - \frac{1}{2}(X_0\cos t + Y_0\sin t)^2 - \frac{1}{3!}(X_0\cos t + Y_0\sin t)^3 \ldots \tag{14.31}$$

with a similar equation for $Y_0(\tau)$. To avoid secular terms in the solution for $x_1(t)$ we demand that all terms proportional to $\cos t$ or $\sin t$ on the right-hand side of Eq. (14.31) (or its y equivalent) vanish, again to avoid a resonance with the terms on the left-hand side. The quadratic terms do not project onto $\cos t$ or $\sin t$ but the cubic terms do. Evaluating the projection integrals (which are of the form $(2\pi)^{-1}\int_0^{2\pi}\cos^2 t \sin^2 t\, dt$) and restoring the dimensions (noting that $\tau = \varepsilon t$) we obtain, after a little algebra, the equation for the slowly varying amplitude

$$\frac{dr^2}{dt} = 2\varepsilon r^2 - \frac{1}{2}r^4, \tag{14.32}$$

where $r^2(\tau) = (X_0^2(\tau) + X_0^2(\tau))/2$. Equation (14.32) is the Landau equation for this problem. The Landau constant is positive. The growth of the amplitude $x^2 + y^2$ is initially exponential, before equilibrating, and is at all times modified by a fast oscillation. Figure 14.4 shows the equilibrated amplitude from a direct numerical integration of Eqs. (14.19) and (14.20), along with the predicted time-averaged equilibrated amplitude $r^2 = 4\varepsilon$. Quantitative agreement is obtained for small ε values.

We still have not derived a Landau equation from the Navier–Stokes equations. For a real-world problem this is generally an arduous task. Indeed, it was 15 years after Landau first proposed the equation that Stuart and Watson [8] were first able to properly derive a Landau equation for a fluid stability problem in plane parallel flow.

If α is positive then it is clear from Eq. (14.18) that supercritical equilibration can readily be achieved. The solution of Eq. (14.18) is obtained by writing it as a linear equation in $|A|^2$, namely

$$\frac{d|A|^{-2}}{dt} + 2\sigma|A|^{-2} = \alpha, \tag{14.33}$$

which leads to

$$|A|^2 = A_0^2 \Big/ \left\{\frac{\alpha}{2\sigma}A_0^2 + \left(1 - \frac{\alpha}{2\sigma}A_0^2\right)e^{-2\sigma t}\right\}, \tag{14.34}$$

where A_0 is its initial value. For large times $|A|^2$ tends to the limit

$$|A|^2 = 2\sigma/\alpha. \tag{14.35}$$

The growth rate σ will be some function of the Reynolds number (or other

controlling parameter), and because we have no reason to expect the first-order terms to vanish, we have that $\sigma = \text{constant} \times (R - R_c) + O(R - R_c)^2$. Hence, the amplitude of the equilibrated value of $|A|$ is proportional to $\sqrt{R - R_c}$. For $R < R_c$ the flow is stable. The bifurcation at $R = R_c$ is a supercritical Hopf bifurcation; it is a bifurcation from a stable fixed point to a limit cycle. For our model problem, Eq. (14.19), direct numerical solution of the original equations confirms the predictions of the weakly nonlinear theory. The averaged value of the equilibrated amplitude squared is, as predicted, a *linear function* of the growth rate ε. Furthermore, the dependence on the cubic term in the nonlinear function f_1 is much stronger than the dependence on the quadratic terms: if the quadratic terms are eliminated the equilibrated amplitude is very similar (Fig. 14.4), whereas if the cubic terms are eliminated, now retaining the second-order terms, the equilibrated values (not shown) are in face quite different.

If α is negative, then for $R < R_c$ there is a stable fixed point surrounded by an unstable limit cycle. The flow is thus metastable, because infinitesimal perturbations are damped back to the focus, but finite size perturbations (which exceed the radius of the limit cycle) are unstable. For $R > R_c$ there is no steady flow (at least to fourth order) because both terms on the right-hand side of Eq. (14.18) are positive and $|A|$ increases very rapidly; higher-order terms must be included for equilibration. In fact, we may hypothesize that after such a "subcritical" Hopf bifurcation the transition to turbulence is very rapid. (Indeed in the Lorenz equations the transition to chaos occurs after a single subcritical Hopf bifurcation [4].)

14.3 From Nonlinear Equilibration to Weak Turbulence

Suppose that the control parameter has been turned up past a first instability and equilibration has occurred, roughly obeying the Landau equation. (Actually, even at this stage, detailed equilibration mechanisms differ. See, for example, Pedlosky [8]). We now have a limit cycle. The question arises: what happens if the control parameter R is increased further. Common experience tells us that, even after a supercritical bifurcation, the limit cycle does not persist (if only turbulence were so simple). One possible scenario, now generally thought false, is the Landau–Hopf picture. After the first bifurcation, the flow is periodic with a frequency f_1 say, and hence is a single point on a Poincaré map. In principle it is possible to perform a stability analysis about this (time-dependent) flow, in much the same way as one performs a stability analysis about a stationary flow (except it is harder). Now, as R increases the periodic motion increases in amplitude, and, it may be supposed, the flow will eventually become unstable (say at R_2). If this instability is caused by a Hopf bifurcation to another limit cycle, then a second frequency, f_2, will be present. There is no reason that f_2 and f_1 be related, so for

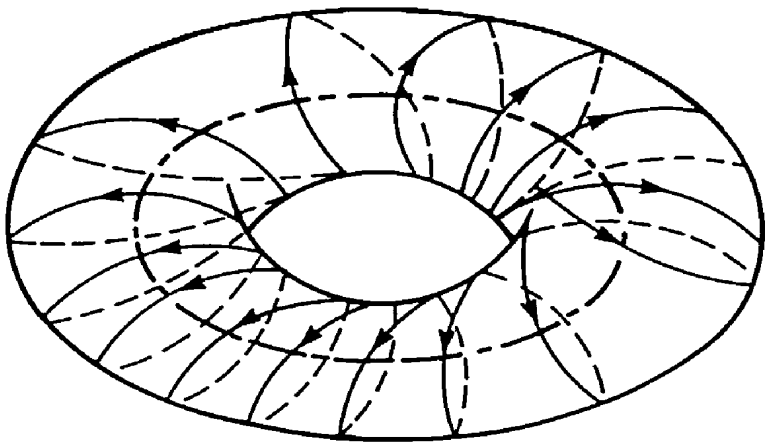

FIGURE 14.5. Motion on a torus. If the path round the torus does not close, the motion is quasiperiodic.

almost all cases f_1/f_2 will be irrational. The flow is then *quasiperiodic* on a torus (Fig. 14.5). Why quasiperiodic? If the flow due to the first frequency is $\phi \sim \exp[if_1 t]$ then the phase of this component will return to its initial value after a time t such that $f_1 t = 2\pi m$ where m is any integer. Similarly the phase of the second flow will return to its initial value after a time $t = 2\pi n/f_2$, where n is another integer. The flow will thus have an overall period $T = 2\pi m/f_1 = 2\pi n/f_2$, requiring $f_1/f_2 = m/n$. But if f_1 and f_2 are irrationally related, no such integers exist. Thus the flow has infinite period. But we can approximate f_1/f_2 as accurately as we wish by the ratio of two integers, so to any desired degree of accuracy the flow may be regarded as periodic.

A third bifurcation will produce another frequency, and so on. Eventually, Landau supposed, after many bifurcations a "turbulent flow," comprising many independent and irrationally related frequencies, arises. Such a picture is false, on both experimental and theoretical grounds. We shall now discuss why, and what in fact does happen. We will discuss only three transition sequences—although more may exist. We will pay most attention to the period-doubling route, partly in the interests of space and partly because the scaling properties are quite transparent here.

14.3.1 The Quasi-Periodic Sequence

The Landau sequence may be schematized as

$$\begin{pmatrix}\text{Steady}\\ \text{flow}\end{pmatrix} \Rightarrow \begin{pmatrix}\text{Periodic}\\ \text{Flow}\end{pmatrix} \Rightarrow \begin{pmatrix}\text{Periodic 2}\\ \text{flow}\end{pmatrix} \Rightarrow \begin{pmatrix}\text{Periodic 3}\\ \text{flow}\end{pmatrix} \Rightarrow \begin{pmatrix}\text{Periodic 4}\\ \text{flow}\end{pmatrix} \cdots,$$

where the arrows denote Hopf bifurcations. Now, a quasiperiodic flow is predictable, meaning it does not display sensitive dependence on initial condi-

tions. This is because quasiperiodic flow is just flow on a torus, and although flow on a torus may be ergodic (i.e., it explores all of the available phase space) the flow is not mixing (two orbits initially close together explore the torus together) and is not unpredictable. However, turbulent flow is known to be unpredictable, and was known to be so before "chaos theory," excepting the work by Poincaré, was discovered [9]. (We discuss predictability properties later in this chapter.) However, it is fair to say that the reasons for its unpredictability were not at that time fully understood. Thus, the Landau picture is not supported by observation or experiment. Theoretically, too, it turns out that quasiperiodic motion is unstable to small perturbations of the equations of motion. Two phenomena occur. First, the addition of a small amount of nonlinearity may lead to frequency locking, in which the independent frequencies become truly rationally related. Second, for larger values of a nonlinearity parameter, the surface of the torus may crinkle, and a strange attractor may arise. This is the "Ruelle–Takens" or "quasiperiodic" route to chaos [10], and the sequence may be characterized as

$$\begin{pmatrix}\text{Steady}\\ \text{Flow}\end{pmatrix} \Rightarrow \begin{pmatrix}\text{Periodic}\\ \text{Flow}\end{pmatrix} \Rightarrow \begin{pmatrix}\text{Periodic 2}\\ \text{flow}\end{pmatrix}\left(\Rightarrow \begin{pmatrix}\text{Periodic 3}\\ \text{flow}\end{pmatrix}\right) \Rightarrow \begin{pmatrix}\text{Strange}\\ \text{Attractor}\end{pmatrix}.$$

The precise number of Hopf bifurcations before chaos emerges is probably not important. The important point is that after a small number of bifurcations a strange attractor generically emerges.

To examine these phenomena, and to keep the analysis tractable, it is unfortunately necessary to keep only the vestiges of the Navier–Stokes equations. The price is that the approach is less deductive than we like; the reward is universality. The simplest model displaying quasiperiodicity is probably the circle map—the map of the circle onto itself

$$\theta_{n+1} = \theta_n + \Omega - \frac{K}{2\pi} \sin 2\pi\theta_n \quad \text{(modulo 1)}. \tag{14.36}$$

If the nonlinearity parameter K is zero then the map displays only two kinds of behavior, periodic for Ω rational and quasiperiodic for Ω irrational. Rational numbers can by definition be expressed as the ratio of two integers, p/q. Although dense (i.e., we can approximate any number arbitrarily closely by a rational) they form a set of zero measure on the real line—which means, loosely, that if we pick a number at random its chances of being rational are zero. Thus, periodic behavior for this map is nongeneric. However, if we add a small amount of nonlinearity, then frequency locking occurs and for a set of Ω of nonzero measure (indicated by the shaded areas in Fig. 14.6) periodic behavior occurs. (Note that for some numbers the quasiperiodic regime persists longer than for other; these numbers are "more irrational," in the sense of the continued fraction representation. The golden mean $(\sqrt{5}-1)/2 = 0.618\ldots$ is the most irrational number in this sense, having entries that are all unity.) For values of K greater than unity chaotic motion may arise.

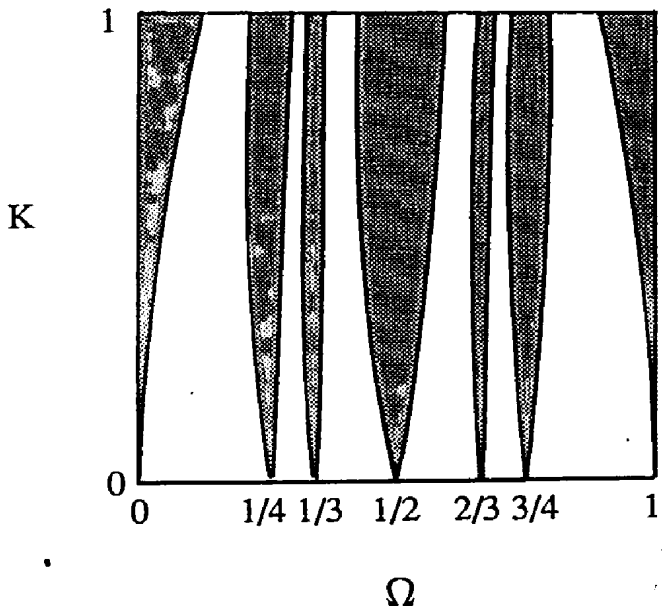

FIGURE 14.6. Frequency locking in the circle map (schema). The shaded regions indicate periodic behavior, for which the parameter region grows as nonlinearity increases. For $K > 1$ chaotic motion may ensue.

14.3.2 The Period Doubling Sequence

This is based on the pitchfork bifurcation. In a pitchfork bifurcation a periodic orbit (which can be replaced by a fixed point using a Poincaré map) is replaced by a periodic orbit of twice the period. A great deal of progress can be made by studying one-dimensional maps of the form:

$$x_{n+1} = f(x_n), \tag{14.37}$$

where $f(x)$ is an analytic function of x. Perhaps the most well known of these is the logistic map

$$f(x) = rx_n(1 - x_n), \tag{14.38}$$

where r plays the role of control parameter. We will study this map is some detail, to get a feeling for the mechanisms of period doubling. After that we will study the universal scaling features of this and similar maps, and apply some simple renormalization group arguments. First we note some general properties of the map Eq. (14.37). The second iterate of the map yields

$$x_{n+2} = f(f(x_n)) = f_2(x_n). \tag{14.39}$$

The nth iterate will be denoted $f_n(x)$. Fixed points of Eq. (14.37) are found by solving

$$x^* = f(x^*).$$

Stability of these is then determined by examining small perturbations around the fixed point. Let

$$x_n = x^* + \varepsilon_n.$$

Then

$$\begin{aligned} x_{n+1} &= f(x_n) = f(x^* + \varepsilon_n) \\ &= f(x^*) + \varepsilon_n f'(x^*) = x^* + \varepsilon_n f'(x^*) \\ &= x^* + \varepsilon_{n+1} \quad \text{(say)}. \end{aligned} \tag{14.40}$$

The error grows if $|\varepsilon_{n+1}/\varepsilon_n| > 1$; thus, the condition for instability is that

$$|f'(x^*)| > 1. \tag{14.41}$$

If a fixed point at x_0 is unstable, then all higher iterates are also unstable at x_0. This is because

$$f_2'(x_0) = f'(x_0)f'(f(x_0)) = f'(x_0)f'(x_1), \tag{14.42}$$

and at the fixed point $x_1 = x_0$, and so

$$f_2'(x^*) = |f'(x^*)|^2. \tag{14.43}$$

In general the slope of the nth iterate is given by a simple extension of Eq. (14.42), namely

$$f_n' = \prod_{i=0}^{n-1} f'(x_i). \tag{14.44}$$

Now, for specificity, consider the logistic map Eq. (14.37). Graphically, the situation is illustrated in Fig. 14.7. The solid curve displays the function Eq. (14.38) and the dashed line is of unit slope (the identity line). To obtain successive iterates pick an initial value, x_0, along the abscissae and move parallel to the ordinate until the function curve is intersected; the ordinate value then gives x_1. Then move horizontally to meet the dashed line, and then vertically again to meet the solid curve, to obtain the next value in the iteration sequence and so on. If $0 < r < 4$ then the function always maps the interval $\{0, 1\}$ to itself. Because the map is quadratic, and therefore with single extremum, there are up to two fixed points, at the origin $x = 0$ and (for $r > 1$) at $x = 1 - 1/r$. These occur where the function crosses the identity line. Their stability is determined by the value of f', and we have

(i) Origin ($x^* = 0$); $f' = r$; and
(ii) $x^* = 1 - 1/r$; $f' = 2 - r$.

For $0 < r < 1$ the origin, being the only fixed point, is stable. Beyond $r = 1$ the fixed point loses its stability and the other fixed point emerges, and for all initial conditions the flow will eventually converge to this fixed point. This

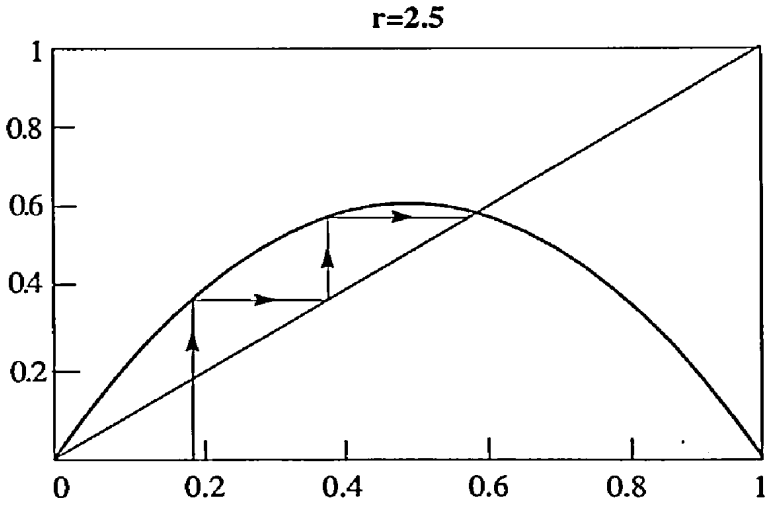

FIGURE 14.7. The logistic map for $r = 2 \cdot 5$. Note the convergence to the stable fixed point from any initial condition.

point itself becomes unstable when

$$|2 - r| > 1 \Rightarrow r = 3. \tag{14.45}$$

Thus for $r > 3$ there are no stable fixed points. What happens?

The answer to this is that the flow bifurcates from a fixed point to a periodic flow (a Period 1 flow). To see this consider the map obtained by iterating Eq. (14.38),

$$\begin{aligned} f_2(x) &= f(f(x)) = r^2x(1-x)(1-rx(1-x)) \\ &= r^2x - (1+r)r^2x^2 + 2r^3x^3 - r^3x^4. \end{aligned} \tag{14.46}$$

Its precise form will not turn out to be too important. However, we note that it is a quartic, with three extrema, symmetrical about and with a minimum at $x = 1/2$. [The positions of the other two minima can be obtained by an application of Eq. (14.42). Because

$$f_2'(x_0) = f'(x_0)f'(x_1), \tag{14.47}$$

there is a zero at x_0 when the point to which it iterates has zero slope. Thus, the points that iterate to $x = 1/2$, that is, $f^{-1}(1/2)$, are maxima of f_2.]

Now, the fixed point of f loses its stability as r increases through $r = R_1 = 3$, with $x = 2/3$. The stability is lost in f_2 also [by Eq. (14.42) or (14.44)]. However, as can be seen from Fig. 14.8, two new (stable) fixed points in f_2 emerge. This is the first pitchfork bifurcation, so-called because the values of the fixed points as r is increased look like a pitchfork (Fig. 14.9). This bifurcation has given rise to the phenomena of period doubling, and the

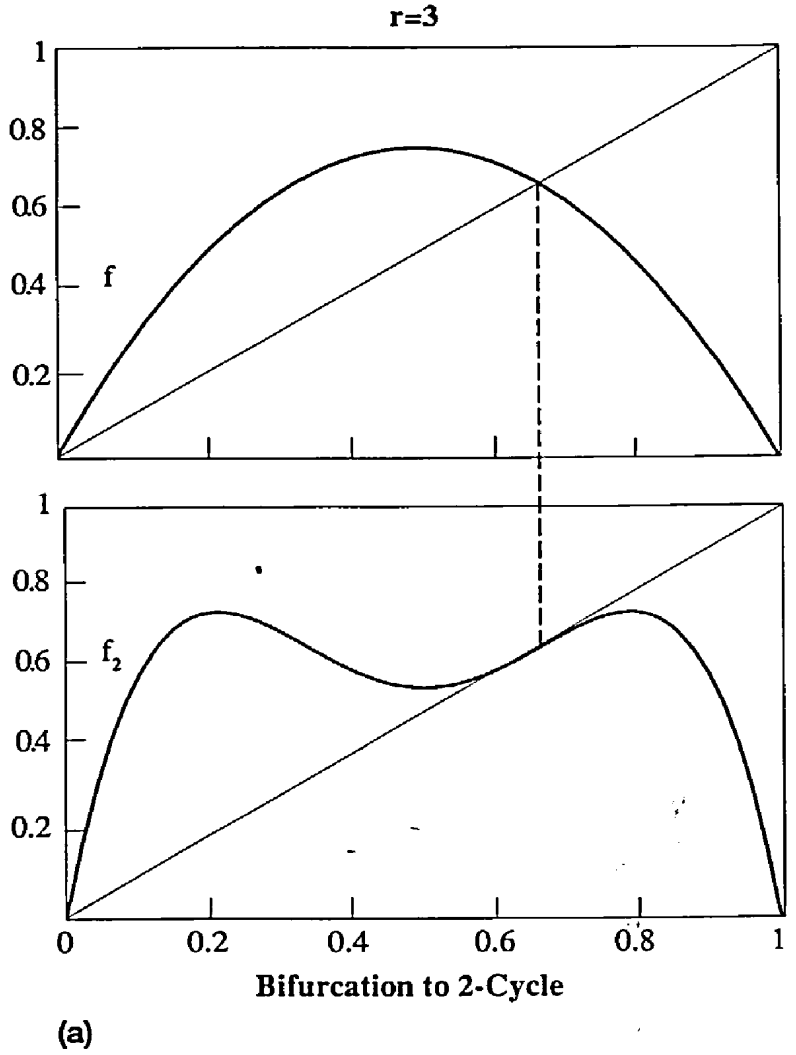

FIGURE 14.8. Period doubling in the logistic map. (a) For $r > 3$ the fixed point of f is unstable.

two new fixed points form a Period 2 flow, or a "2-cycle." The slopes of these two point are the same. We can see this because the actual iteration oscillates between them:

$$\begin{aligned} x_1 &= f(x_0) \\ x_0 &= f(x_1). \end{aligned} \tag{14.48}$$

Thus, using Eq. (14.47),

$$f_2'(x_0) = f'(x_0)f'(x_1) = f_2'(x_1). \tag{14.49}$$

Indeed in general if the set of points $\{x_i\}$ forms an n-cycle such that for each i

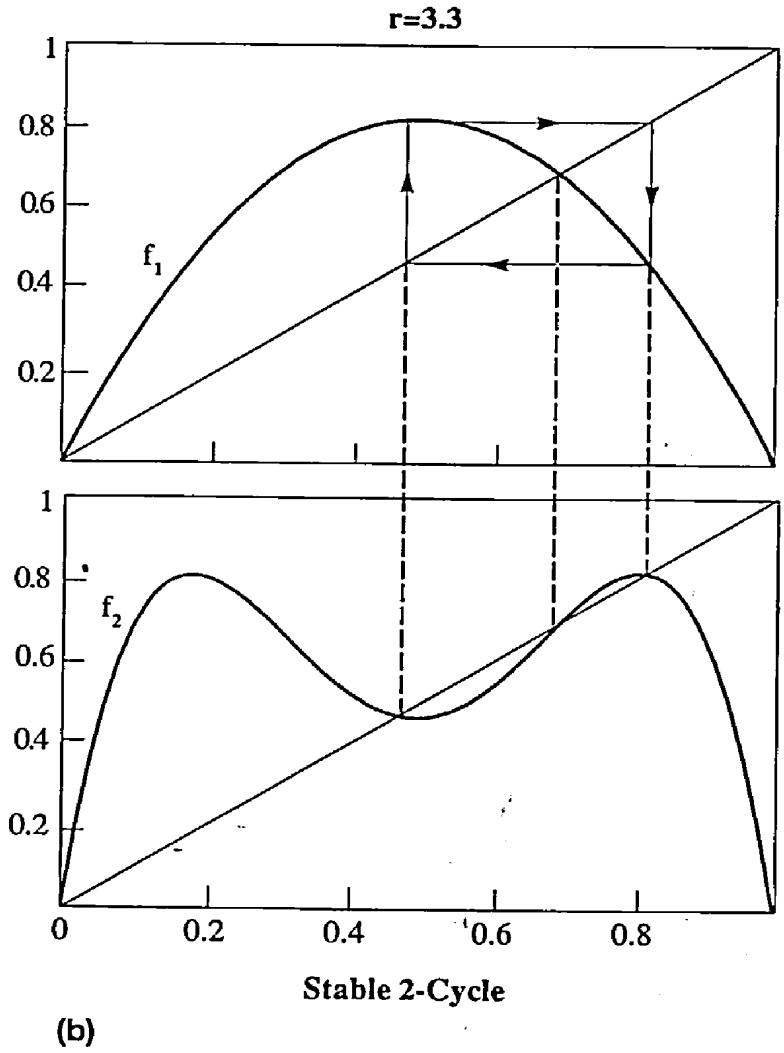

FIGURE 14.8 *(continued)*. (b) For $r = 3.3$ the 2-cycle is stable.

$$x_i^* = f_n(x_i^*) \tag{14.50}$$

then each fixed point has the same slope in the f_n map, given by

$$f_n' = \prod_{i=1}^{n} f'(x_i^*). \tag{14.51}$$

For r marginally bigger than R_1, the two new fixed points are very close together, and consequently their slopes are less than unity and they are stable. However, as r increases they move further apart, passing through a so-called superstable cycle when the slopes of the slopes of the fixed points of f_2 are zero. At a particular value of r, in fact at $r = R_2 = (1 + \sqrt{6}) = 3.4495$, their slopes become greater in magnitude than -1 and another pitchfork bifurcation gives rise to four new stable fixed points, and Period 4 flow. Note that the

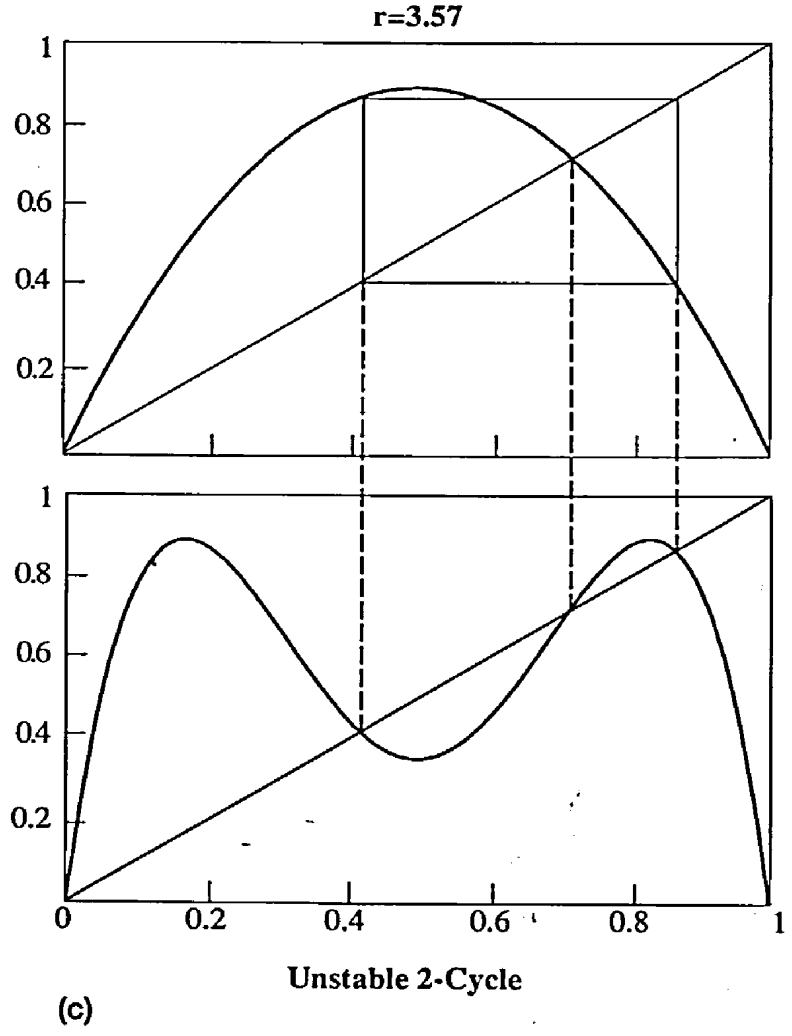

FIGURE 14.8 *(continued).* (c) For $r > 1 + \sqrt{6}$ the 2-cycle is unstable. For $r = 3.57$ (illustrated) the absolute value of the slope of f_2 is clearly greater than unity.

pitchfork bifurcations occur simultaneously because it is a single trajectory that is being split, and the slopes at each of the fixed points are the same. These new fixed points eventually become unstable and bifurcate to a Period 8 flow, and so on in a period-doubling sequence. The successive bifurcations occur closer and closer together, in a geometric progression, and eventually accumulate at some particular value of r, denoted R_∞, whose value is 3.5699456 for the logistic map. For $r > R_\infty$ the iteration sequence is chaotic.

Scaling and Universality

If one numerically integrates the logistic map and notes the values of r at which successive bifurcations occur (R_1, R_2, etc.) then one finds that the ratio

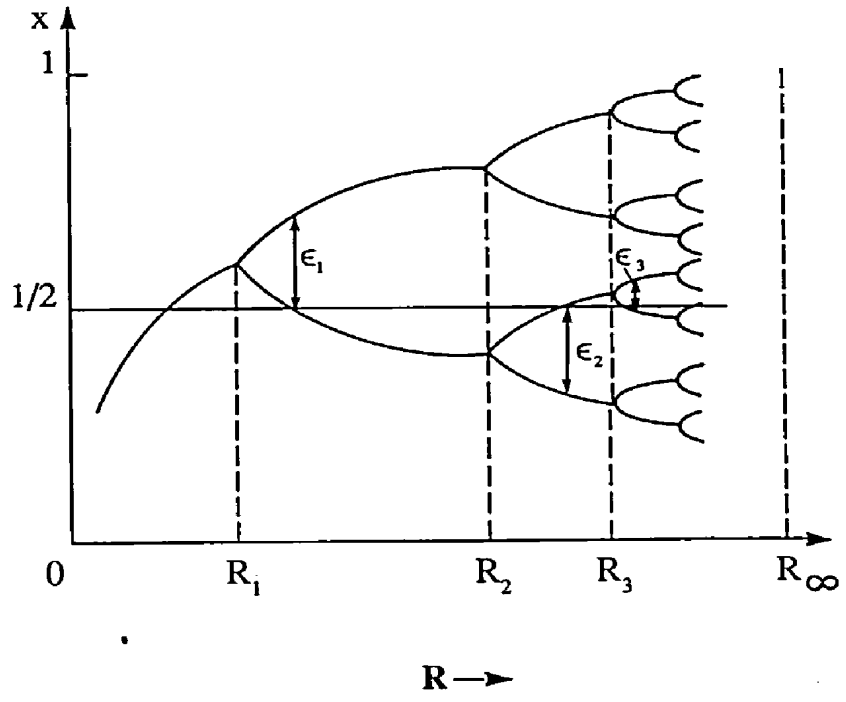

FIGURE 14.9. Pitchfork bifurcations in the logistic map. The ordinate gives the values of successive iterations. For $R > R_\infty$ the mapping is chaotic.

of intervals between bifurcations tends to a limit:

$$\delta = \lim_{n\to\infty} \frac{R_n - R_{n-1}}{R_{n+1} - R_n} = 4.6692. \tag{14.52a}$$

Because

$$\lim_{n\to\infty} \frac{R_\infty - R_n}{R_\infty - R_{n+1}} = \lim_{n\to\infty} \frac{R_\infty - R_{n-1}}{R_\infty - R_n},$$

then Eq. (14.52a) is equivalent to

$$\delta = \lim_{n\to\infty} \frac{R_\infty - R_n}{R_\infty - R_{n+1}} = 4.6692. \tag{14.52b}$$

Furthermore, the relative scale of branch splittings (see Fig. 14.9) is also universal:

$$\alpha = \lim_{n\to\infty} \frac{\varepsilon_n}{\varepsilon_{i+1}} = 2.503. \tag{14.53}$$

Here α essentially measures the reduction in scale that follows each bifurcation. These parameters are *universal*, in the sense that their values do not depend on the particular map (except that it be quadratic) and the ratios hold

(in the limit $n \to \infty$) for every bifurcation. Let us try to understand why this should be, before trying to deduce their values.

It is convenient to transform the logistic map Eq. (14.38) first by the shift $x \Rightarrow x + 1/2$ and then by $x \Rightarrow x(r/2 - 1)/2$. These then yield the map

$$x_{n+1} = 1 - \lambda x_n^2. \tag{14.54}$$

where

$$\lambda = \frac{r}{2}\left(\frac{r}{2} - 1\right). \tag{14.55}$$

The map is centered at $x = 0$ and is such that if $0 < \lambda < 2$ then $-1 < x < 1$. The fixed points of this are determined by $\lambda x^2 + x - 1 = 0$, which become unstable [by Eq. (14.41)] when $2\lambda x = 1$, giving $\lambda = 3/4$ (and $x = 2/3$). Thus the first bifurcation occurs at $\lambda = \Lambda_1 = 3/4$. Iterating the transformation gives

$$f_2 = x_{n+2} = 1 - \lambda + 2\lambda^2 x_n^2 - \lambda^3 x^4. \tag{14.56}$$

Neglecting the quartic term, and rescaling by $x \Rightarrow x/\alpha$ we obtain

$$x_{n+2} = 1 + 2\lambda^2(1 - \lambda)x_n^2 = 1 - \lambda_1 x_n^2, \tag{14.57}$$

which is of the same form as Eq. (14.54) but with

$$\lambda_1 = \phi(\lambda) = 2\lambda^2(\lambda - 1). \tag{14.58}$$

Successive iterations of this map then yield

$$x_{n+2^m} = 1 - \lambda_m x_n^2 \qquad \lambda_m = \phi(\lambda_{m-1}). \tag{14.59}$$

Now, the first bifurcation occurs when $\lambda = \Lambda_1 = 3/4$; the next bifurcation (denoted by $\lambda = \Lambda_2$) occurs when $\lambda_1 = 3/4$; that is, when $\phi(\Lambda_2) = \Lambda_1$. The bifurcation after that occurs when $\phi(\phi(\Lambda_3)) = \Lambda_1$; that is, when $\phi(\Lambda_3) = (\Lambda_2)$. Thus, the sequence of bifurcations is calculated by the sequence:

$$\Lambda_1 = \tfrac{3}{4}, \quad \phi(\Lambda_2) = \Lambda_1, \quad \phi(\Lambda_3) = \Lambda_2 \ldots \tag{14.60}$$

These are easily calculated to be at 0.75, 1.2428, 1.3440, 1.3622, 1.3654, 1.3659, 1.3660,... The bifurcations *accumulate* at the fixed point given by $\Lambda_\infty = \phi(\Lambda_\infty)$ giving $\Lambda_\infty = (1 + \sqrt{3})/2 = 1.3660$. This is to be compared to the exact value 1.4011 obtained by a direct solution of Eq. (14.54). [Using Eq. (14.55), we obtain the accumulation point for the map in its more common form (14.38), $R_\infty = 3.54246$, whereas the exact value is 3.56994]. The value of Λ_∞ is not universal, being dependent on how the map is specifically defined. However, the scale factors α_m tend in the limit $n \to \infty$ to $\alpha_m = 1/(1 - \Lambda_\infty) = -2.73$ (cf. the exact value $\alpha = -2.5029$). We can also estimate the ratio of

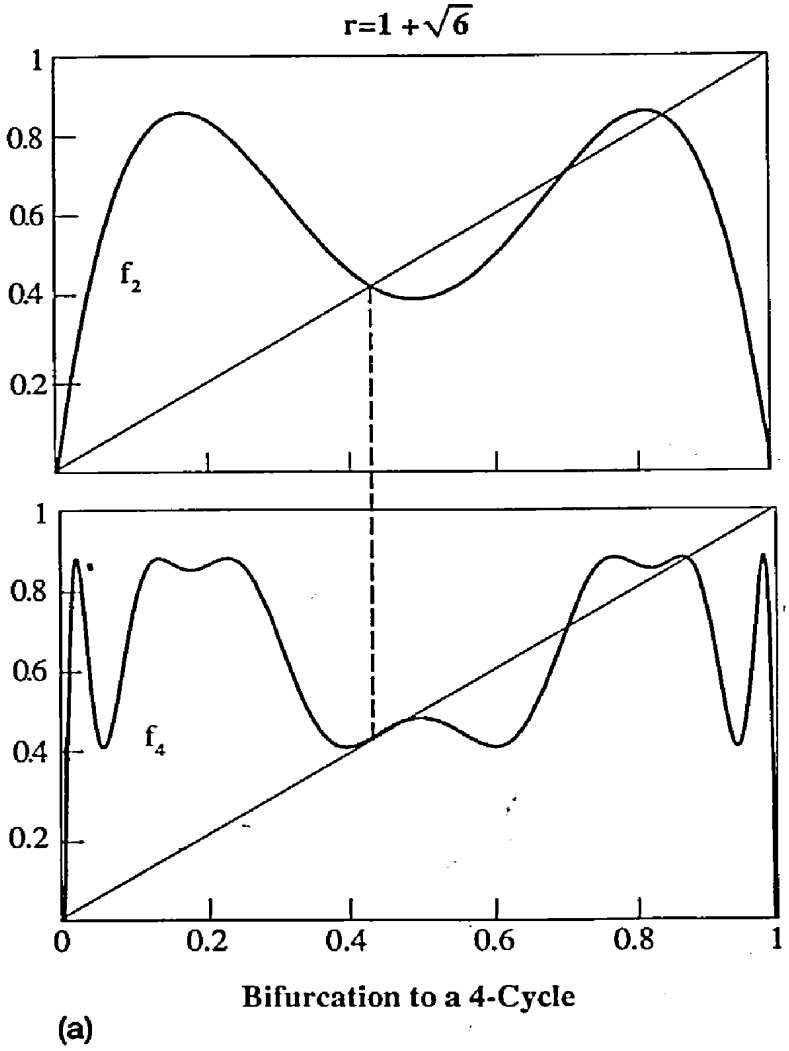

FIGURE 14.10. From Period 2 to Period 4. (a) At $r = 1 + \sqrt{6}$ the 2-cycle becomes unstable.

bifurcation intervals, as follows. Using Eq. (14.60) in the limit $m \to \infty$ we have

$$\begin{aligned} \Lambda_\infty - \Lambda_m &= \Lambda_\infty - \phi(\Lambda_{m+1})' \\ &\approx \Lambda_\infty - \{\phi'(\Lambda_\infty)(\Lambda_{m+1} - \Lambda_\infty) + \phi(\Lambda_\infty)\} \\ &= (\Lambda_\infty - \Lambda_{m+1})\phi'(\Lambda_\infty) \end{aligned} \tag{14.61}$$

Hence

$$\delta = \phi'(\Lambda_\infty) = \lim_{m\to\infty} \frac{\Lambda_\infty - \Lambda_m}{\Lambda_\infty - \Lambda_{m+1}}. \tag{14.62}$$

For our simple approximations, this gives the value $\delta = 4 + \sqrt{3} = 5.732$, which is within 25% of the exact value. It is becoming clearer now why these

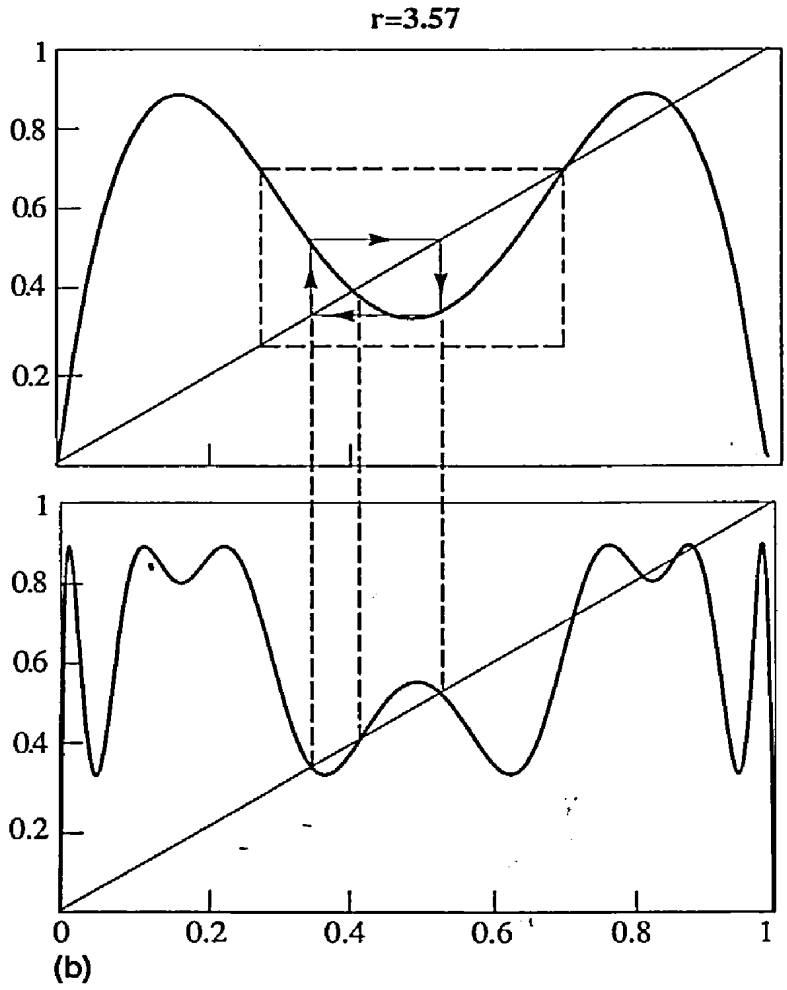

FIGURE 14.10 *(Continued).* (b) The 4-cycle is unstable (as indeed are all higher iterates) at $r = 3.57$. Note that the inverse of the center portion (dashed) of (b) is very similar to the entirety of Fig. 14.8 (c). This is a characteristic of universality.

values are universal (see also Fig. 14.10). After each bifurcation the values of the iterated map f_m in the range $[-1, 1]$ are determined by the values of f_m in a part of the range smaller by a factor α. After many iterations, the determination of the iterated function is determined by the initial function closer and closer to its maximum. If the maximum of f_0 (the initial map) is quadratic, this fact alone suffices to determine α and δ.

The General Doubling Transformation

Rather than truncate the map after each bifurcation to keep its quadratic form, we will try now to be a little more general. Consider the mapping $f_1(x; \lambda)$ such that $f(0) = 1$. Equation (14.54) is an example of this. Then the iterated map is $f_2 = f(f(x; \lambda))$. However, the previous discussion suggests

we rescale with the factor $\alpha_1 = 1/f_1(1)$ to obtain

$$f_2(x) = \alpha_1 f_1[f_1(x/\alpha_1)], \quad \alpha_1 = \frac{1}{f_1(1)}.$$

Further transformations yield the sequence

$$f_{n+1}(x) = Tf_n(x) = \alpha_n f_n[f_n(x/\alpha_n)], \quad \alpha_n = \frac{1}{f_n(1)}, \tag{14.63}$$

where T is known as the "doubling operator." In the limit of $n \to \infty$ this sequence tends to a unique limit, and the functional fixed point of the doubling operator satisfies

$$g(x) = \alpha g[g(x/\alpha)], \quad g(0) = 1. \tag{14.64}$$

This is a so-called "functional renormalisation group" equation. Such a function does exist, although it cannot be written in a closed form with a finite number of terms. It is an even function, because it may be obtained as an iteration of an initially even function $f_0(x)$, and it has an infinite number of extrema. If g is known, then the universal scale factor α is given by

$$\alpha = \frac{g(0)}{g[g(0)]} = \frac{1}{g(1)}. \tag{14.65}$$

We can obtain approximate solutions to Eq (14.64) by substituting even polynomial expansions for g. The simplest such solution is given by setting

$$g(x) = 1 + mx^2. \tag{14.66}$$

Then Eq. (14.64) gives

$$1 + mx^2 = \alpha[1 + m(1 + m(x/\alpha)^2)^2]. \tag{14.67}$$

Equating powers of x gives $\alpha = 1/(1 + m)$ and $\alpha = 2m$ yielding the numerical values

$$m = -(1 + \sqrt{3})/2 = -1.366, \quad \alpha = (1 + \sqrt{3}). \tag{14.68}$$

Going to the next order, we set $g(x) = 1 + mx^2 + nx^4$. Substituting into Eq. (14.64) we obtain

$$m = -1.52224, \quad n = 0.127613, \quad \alpha = -2.53404. \tag{14.69}$$

These are quite close to the exact values [11]:

$$\begin{aligned} g(x) &= 1 - 1.52763x^2 + 0.104815x^4 - 0.0267057x^6 \ldots \\ \alpha &= -2.5029 \ldots \end{aligned} \tag{14.70}$$

[To obtain a polynomial expansion it is easiest just to iterate the sequence (14.63), rather than to assume a polynomial expansion with unknown coefficients and substitute in (14.69) to obtain their values.] Finally, we may

obtain accurate values of δ by linearizing around the universal function $g(x)$. Close to the fixed point we may write

$$g_\varepsilon = g(x) + \varepsilon h(x). \tag{14.71}$$

Then

$$\begin{aligned} g_\varepsilon(g_\varepsilon(x)) &= g_\varepsilon(g(x)) + \varepsilon h(x)) \\ &\approx g(g(x)) + \varepsilon g'(g(x))h(x) + h(gx))]. \end{aligned} \tag{14.72}$$

And the universal equation for δ is [11]:

$$g'(g(x)h(x) + h(g(x)) = -\frac{\delta}{\alpha}h(\alpha x). \tag{14.73}$$

Because $g(x)$ and α are already known, we can solve this to any desired accuracy by substituting a polynomial expansion, to obtain $\delta = 4.66920\ldots$.

Summarizing the period-doubling sequence we have then

$$\begin{pmatrix}\text{Steady}\\ \text{flow}\end{pmatrix} \Rightarrow \begin{pmatrix}\text{Periodic}\\ \text{Flow}\end{pmatrix} \rightarrow \begin{pmatrix}\text{Period 2}\\ \text{flow}\end{pmatrix} \rightarrow \begin{pmatrix}\text{Period 4}\\ \text{flow}\end{pmatrix} \rightarrow \begin{pmatrix}\text{Strange}\\ \text{Attractor}\end{pmatrix} \cdots,$$

where the first bifurcation is typically of the Hopf type, with subsequent bifurcations being pitchfork or period-doubling.

There is one other sequence we shall discuss, albeit rather briefly, before trying to figure out what all this has to do with fluids.

14.3.3 The Intermittent Sequence

For this sequence we return to the one dimensional map. Suppose that the an appropriate map (which governs the orbit) has, in some region, two intersections with the 45° line (Fig. 14.11). In this diagram the left-most intersection is an attracting fixed point and the right-most one is a repellor. As our control parameter varies, suppose the map effectively moves to the left, and undergoes a *tangent bifurcation*. When the map is just tangent, the intersection is an attracting fixed point that immediately disappears just after the bifurcation. Consider now some initial conditions far from x_0, just after the tangent bifurcation, but still in its prior "basin of attraction." The orbit will still converge toward x_0, because it does not realize yet that the fixed point is no more. The system then spends many iterations close to the pseudo-fixed point, before wandering away. The tangent bifurcation has replaced an attracting fixed point by a strange attractor, but one in which the system spends a lot of time near the pseudo-fixed point. This route is called the intermittent sequence because for many iterations the map is close to the pseudo-fixed point, undergoing motion that is very close to periodic—remember that at the fixed point motion is periodic, having been reduced to a point via a Poincaré map. The system will occasionally wander away from the pseudo-fixed point, undergoing truly chaotic (broad-band) motion, or intermittent

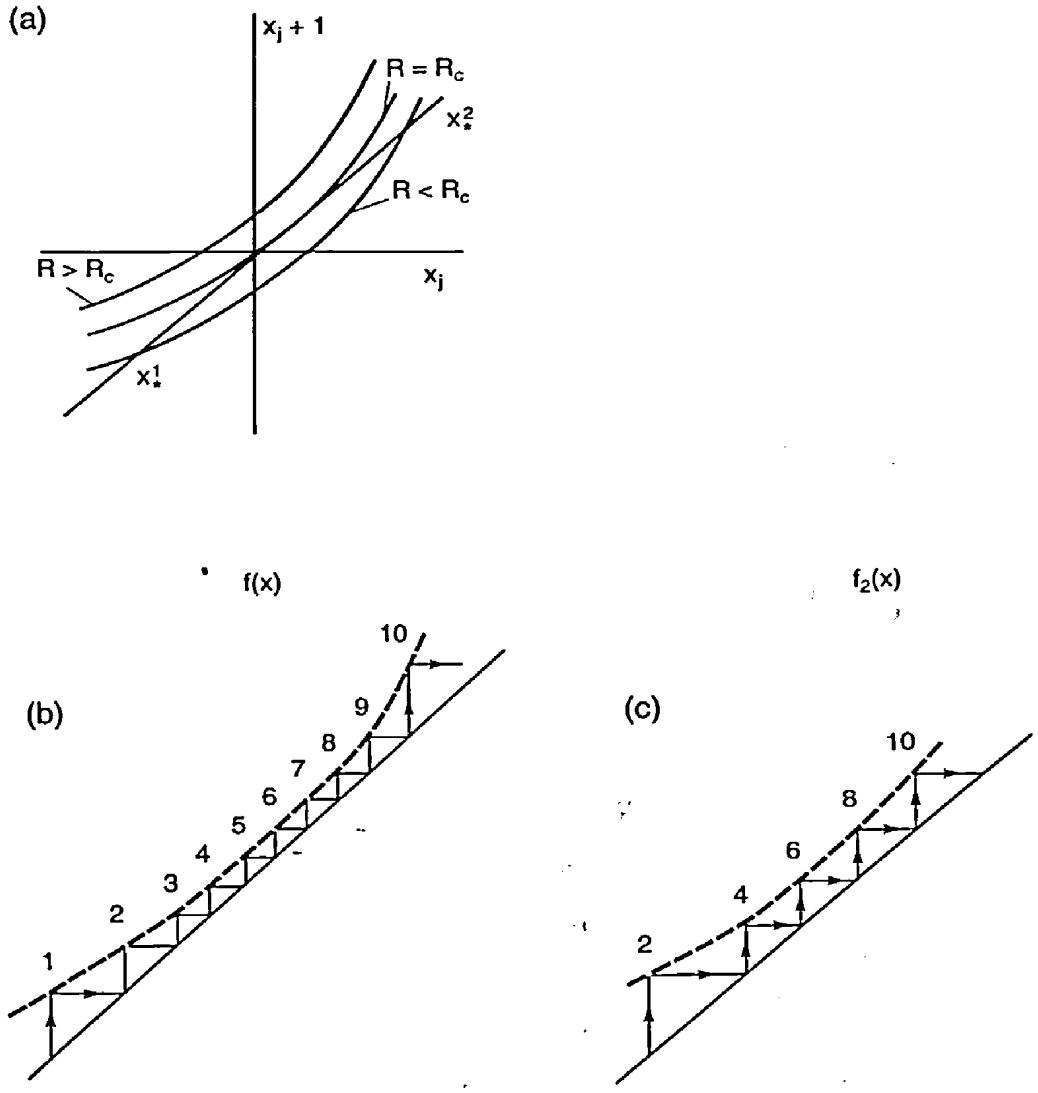

FIGURE 14.11. A tangent bifurcation. Two fixed points merge and then disappear, giving rise to intermittent chaos. The similarity of f_1 and f_2 give rise to universality.

bursts of turbulence. The bifurcation sequence may be summarized as

$$\begin{pmatrix}\text{Steady}\\ \text{flow}\end{pmatrix} \Rightarrow \begin{pmatrix}\text{Periodic}\\ \text{Flow}\end{pmatrix}' \rightarrow \begin{pmatrix}\text{Intermittent}\\ \text{chaotic flow}\end{pmatrix},$$

where the bifurcation to the strange attractor is the tangent bifurcation.

This sequence too displays universal behavior [12]. Close to the tangent fixed point, the function $f(x)$ and its iterate $f(f(x))$ are rather similar, except that the steps in the iterated map are twice as long. Let us express this self-similarity by the equation

$$g(x) = \alpha g(g(x/\alpha)), \tag{14.74}$$

where $\alpha = 2$. This differs from Eq. (14.64) in that an extra tangency condition must be imposed; namely, $g'(0) = 1$ as well as $g(0) = 0$. We now find

$$g(x) = \frac{x}{1 - rx}, \tag{14.75}$$

where r is arbitrary. The parameter convergence ratio can be found in a similar way to that used in the period doubling case, yielding $\delta = 4$. Now, if the control parameter R increases such that we move $1/\delta = 1/4$ time closer to the fixed point ($R = R_c$), the system stays twice as long (because $\alpha = 2$) near to the pseudo-fixed point. Thus, the average length of periodic motion τ_p scales as

$$\tau_p \sim \frac{1}{(R - R_c)^{1/2}}, \tag{14.76}$$

and therefore decreases as the supercriticality increases.

Another way to see this result is as follows. Near the critical point $R = R_c$ we may suppose that the mapping function can be approximated by

$$x_{n+1} = (R - R_c) + x_n + x_n^2, \tag{14.77}$$

which we approximate by

$$\frac{dx}{dt} = R - R_c + x^2. \tag{14.78}$$

Integrating this between two points on either side of the pseudo-fixed point yields the time taken for the passage between those two points, namely

$$\begin{aligned} \tau_p &= \frac{1}{(R - R_c)^{1/2}} [\tan^{-1}(x/(R - R_c)^{1/2}]_{x_1}^{x_2} \\ &\sim \frac{1}{(R - R_c)^{1/2}}. \end{aligned} \tag{14.79}$$

14.3.4 Fluid Relevance and Experimental Evidence

It is perhaps remarkable that anything in the above few sections has anything at all to do with fluids, yet a number of experiments and simulations have reproduced various of these sequences. Let's first try to figure out why this should be, before mentioning the actual experiments.

The obvious first question to ask is: When and why does a fluid behave like a one-dimensional map? Now, a fluid, although multidimensional, is dissipative; the Navier–Stokes equations are of the form

$$\frac{\partial \mathbf{u}}{\partial t} + \text{Nonlinear and Pressure Terms} = \nu \nabla^2 \mathbf{u}.$$

This means its phase space volume shrinks (for example, for each Fourier component of the velocity field, u_K, we have that $\partial \dot{u}_k / \partial u_k < 0$). If the flow is

chaotic, the flow is stretching and folding in some directions, while shrinking in others. Thus, the dimensionality of the flow is constantly reduced until it is on its attractor. Because the attractor has been produced in this complex way it is both thin and complicated. Prior to chaos, its dimension may be quite small (order unity), and hence in some instances ideas from mapping theory may apply [13]. This qualitative, but probably essentially correct, argument nevertheless cannot be proven to hold (say by a series of rational approximations of the Navier–Stokes equation) in general for a given arbitrary fluid dynamical instability. Thus, there are many unknowns, and it is unclear precisely when any particular transition sequence will occur.

It is the *universality* of the sequences that gives rise to their robustness. For example, the period-doubling sequence of Feigenbaum is by no means unique to the logistic map. Most one-dimensional maps with a hump in the middle will give quantitatively the same behavior (this is why the behavior is called universal). What are the experimental signatures of a period-doubling cascade [14]? Suppose we heat a liquid from below in a low aspect ratio container. If the heating is too small, a balance between heating and heat diffusion is stable, and there is no motion. As the Rayleigh number increases (by making the heating more intense), convection begins, and if the geometry is appropriate two convective rolls appear. A probe measuring temperature at any given point would still, however, give a constant reading, and hence the flow corresponds to an attracting fixed point. As the temperature of the lower surface is slowly increased (by slowly we mean that at each value of the temperature the fluid is allowed to come to an equilibrium), then at some critical value the rolls become unstable to a wave propagating along the roll axis. At any particular Rayleigh number in this regime a probe in the fluid would reveal a single sinusoid; a power spectrum would yield a single frequency f, or single period T. The trajectory of the system in its phase space is a single closed loop (Fig. 14.12). Further increasing the temperature contrast, a new oscillatory mode (wave) appears, superimposed on the original one. Examining the phase space trajectory would reveal a double loop, which only exactly repeats after two cycles. A Fourier analysis would reveal the presence of a second sinusoid, at *double the original period.* This is the first period doubling. How does this look like a pitchfork? Well, for each value of the control parameter (e.g., the Rayleigh number) plot each maximum and minimum value of the temperature. For a single loop there are two such values, for a double loop two maxima and two minima and so on. When plotted this way, each period doubling bifurcation looks like a pitchfork. Note that the energy in the second mode is less than that in the original (note that from a distance the phase space trajectory still looks like a single loop), just as the amplitude of the branch splittings gets smaller with each successive bifurcation on the one-dimensional maps.

Increasing the temperature a little further, the trajectory splits again. Another period doubling bifurcation has occurred, and the phase space trajectory turns into a quadruple loop. The Fourier spectrum shows the domi-

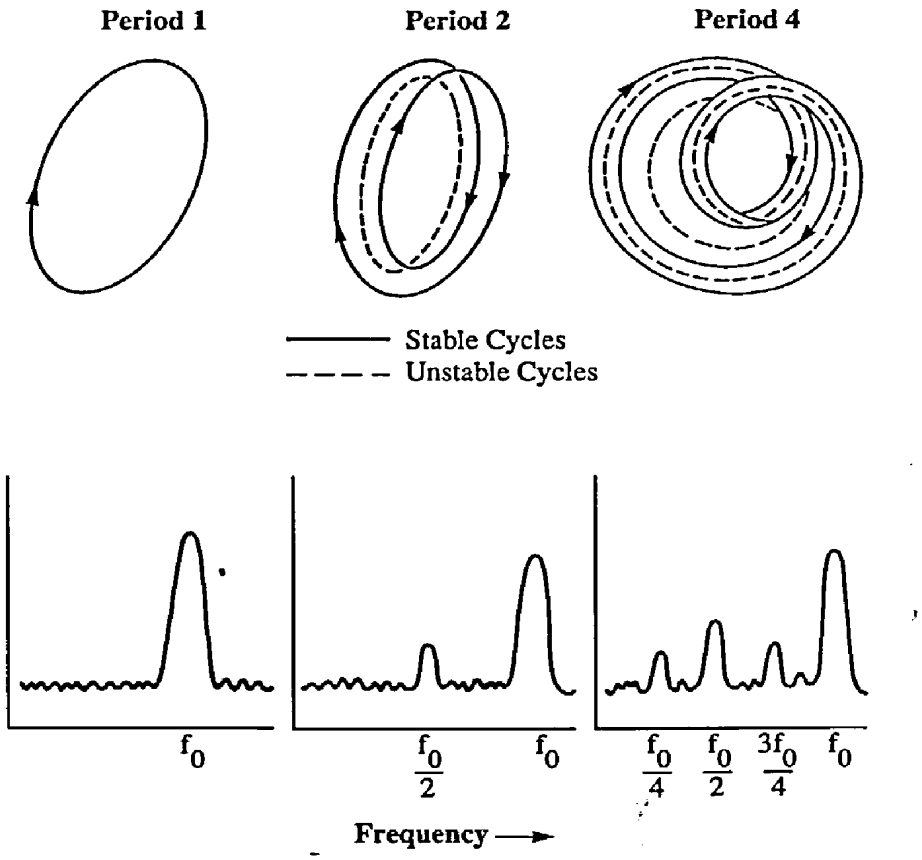

FIGURE 14.12. Period doubling. The upper row illustrates the trajectories in phase space, as the period doubles and then quadruples. The lower row is a schema of the corresponding frequency spectra.

nant scale is still at f, with a weaker contribution at $f/2$ (the doubled period) and a still weaker contribution at $f/4$ and a $3f/4$ harmonic. Ideally, we would be able to see still more period doublings, but it is very hard to discern them, as they they get closer and closer together as a function of Rayleigh number, just as the theory predicts. Period doubling has also been obtained in numerical experiments in two-dimensional convection [15].

The quasiperiodic route has also been observed in a number of hydrodynamical experiments. The experimentalist's goal here is to increase the control parameter slowly, and at closely spaced values obtain a frequency spectra (Fig. 14.13). The signature of this route would then be the appearance of one, two, and perhaps even three or four independent frequencies, after which the flow becomes chaotic and the spectral signature is broad-band. In the experiments of Gollub and Benson [14] two apparently incommensurate frequencies arose, f_1 and f_2, followed by frequency locking with $f_1/f_2 \approx 9/4$. Broadband spectra, a typical signature (although not a proof) of chaos then appeared, with f_1 and f_2 still very visible. This was followed by strongly

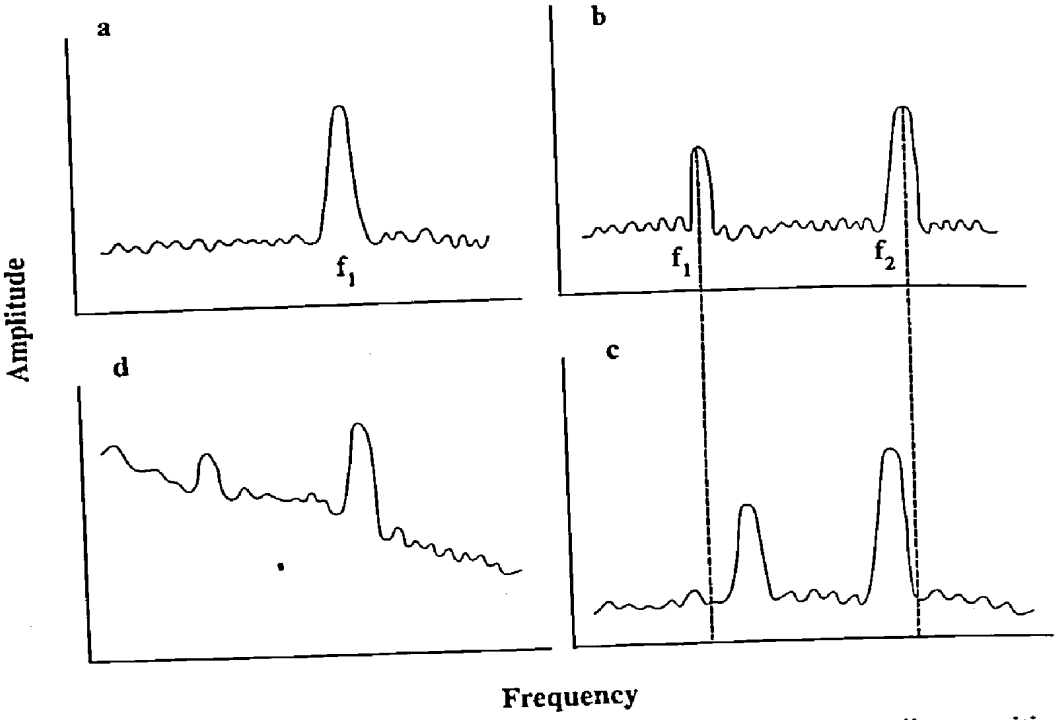

FIGURE 14.13. Schema of frequency spectra for the quasiperiodic transition sequence. In (a) the spectrum is dominated by a single frequency, f_1. In (b) a second incommensurate frequency appears, and in Panel (c) freqencies are locked, by a small shift from their initial values. Another bifurcation brings chaos and a broad-band spectra, in (d).

chaotic flow, with the initial frequencies largely subsumed by the turbulence. Of course it may very difficult for the experimentalist to differentiate this sequence from the appearance of more and more independent frequencies (quasiperiodic flow), which in the presence of a small amount of experimental noise may also have a broad-band spectrum, and very careful experimentation is needed to overcome this. Finally, intermittency has also been observed in experiments [16, 17]. Figure 14.14 schematically illustrates a typical time-series. Note that the intermittency predicted by this Pomeau–Manneville mechanism has no obvious connection with the intermittency observed in strong turbulence, although of course this is not to say one does not exist.

The experimental support for these routes is fairly conclusive evidence for the existence of chaos and strange attractors in weak turbulence. It would be surprising indeed if, after passing through one of a number of fairly well-understood transition sequences, which all imply chaos with all its ramifications, the subsequent passage to strong turbulence occurred via some sequence through which the chaos were removed. Although this is not a proof that chaos exists in turbulence, the question now of much more interest to the physicist is: What good does it do me knowing there is a strange attractor in turbulence?

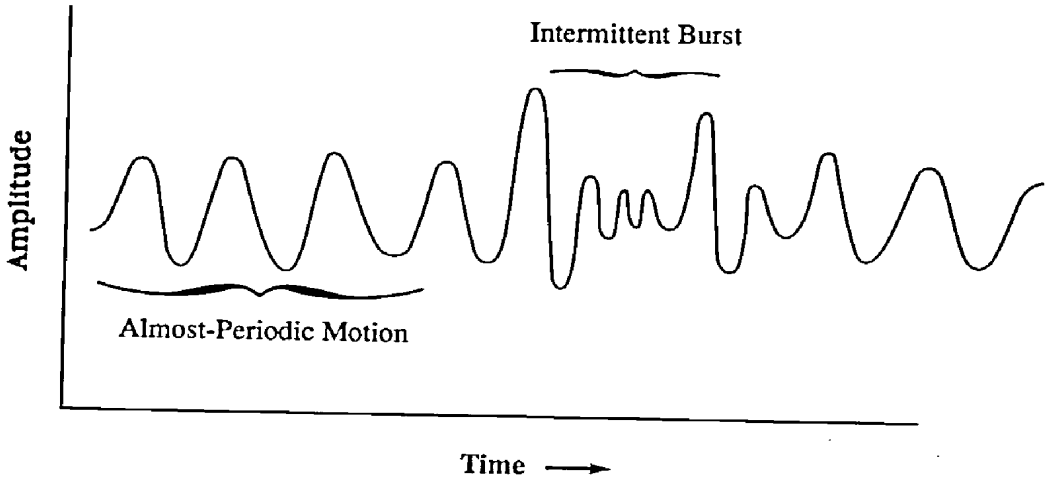

FIGURE 14.14. Schema of an intermittent time series. Periodic flows, when the flow orbits close to a pseudo-fixed point, are separated by bursts of turbulence.

14.4 Strong Turbulence

14.4.1 Scaling Arguments for Inertial Ranges

We will skip over the little-understood area of the transition from low-order chaos to fully developed turbulence, and for the remainder of the chapter focus on fully developed or strong turbulence. Much of the "modern" (say post-1940) theories of this area have foundations made of the scaling arguments of Kolmogorov [18]. For simplicity consider homogeneous, isotropic turbulence in a fluid of constant, unit, density. Suppose that energy is input into the fluid at some length scale L_I, by a stirring process, and a typical resulting velocity is U. The ratio of the inertial terms to the nonlinear terms is the Reynolds number $Re = UL_I/\nu$. If this is large (and just by stirring vigorously we can make it large), there is no effective means of removing energy at the input scale. We may nevertheless expect there to exist some much smaller scale, say $L_D \ll L_I$, at which the Reynolds number (based on L_D and the velocity at that scale) is close to unity, and hence for there to be energy removal at that scale. Thus, energy must be transferred from the larger scales to the smaller scales, for which nonlinearity is necessary. If the stirring is vigorous enough, the input and dissipation scales will be spectrally far removed, and there will exist a range of intermediate scales for which neither stirring or dissipation explicitly is important. This assumption, known as the locality hypothesis, depends on the nonlinear transfer of energy being sufficiently local (in spectral space). Given this, this intermediate range is known as the inertial range. If the stirring produces an energy source of magnitude ε then in a statistically steady state the flux of energy through the inertial range and the dissipation must both equal ε (see Fig. 14.15). All the dynamical fields may be

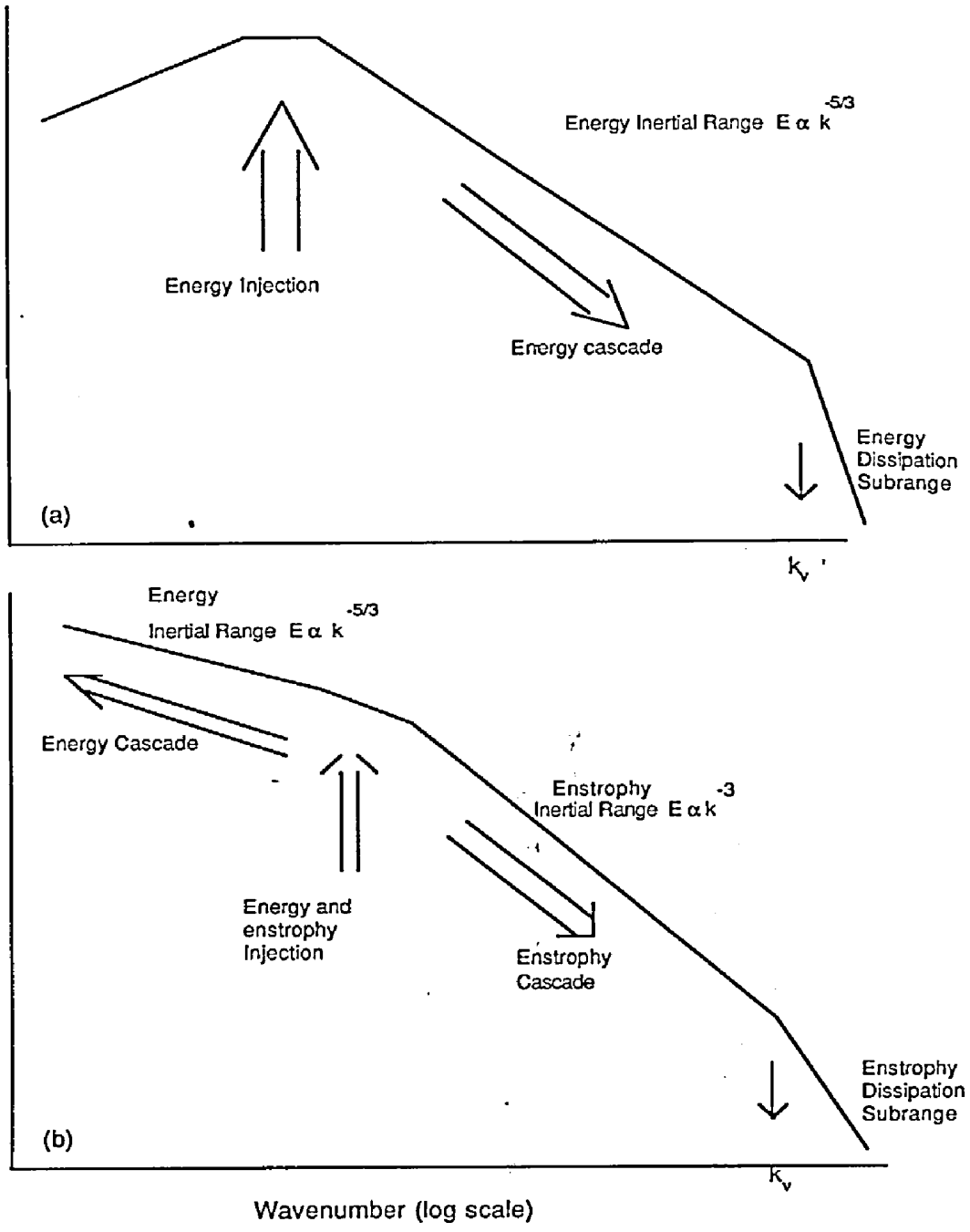

FIGURE 14.15. The putative energy and enstrophy cascades in three-dimensional (a) and (b) two-dimensional turbulence. The ordinate is energy (log scale) and abscissae wave number. The various subranges in reality blend smoothly together.

Fourier decomposed, and denoting the amplitude of the wavenumber by k, we may define an energy spectrum $\mathscr{E}(k)$ such that that the total energy $E = \frac{1}{2}\int \mathbf{u}^2\, d\mathbf{x}$ (remember the density is unity) is given by

$$E = \int_0^\infty \mathscr{E}(k)dk. \tag{14.80}$$

We will also denote a velocity magnitude at a scale $l \sim 1/k$ by v_l or $v(k)$, so that $\mathscr{E}(k) \sim v(k)/k$. This is also a useful stage at which to note that Eqs. (14.1) and (14.2), in the absence of viscosity, conserve the total energy. Simple scaling arguments will now be used to give a relationship between $\mathscr{E}(k)$ and ε.

In the inertial range, the energy transfer is constant and cannot depend explicitly on wave number. The energy spectrum cannot depend on the particular stirring and dissipation processes, because the energy transfer is local. Thus, the energy spectrum $\mathscr{E}(k)$ is a universal function of ε and wavenumber (what else is there?). To obtain the actual functional relationship, it is convenient to define an eddy turnover time $\tau(k)$, which is the time taken for a parcel with energy $\mathscr{E}(k)$ to move a distance $1/k$. Thus,

$$\tau(k) = (k^3\mathscr{E}(k))^{-1/2}. \tag{14.81}$$

Kolmogorov's assumptions are then equivalent to setting

$$\varepsilon \sim \frac{k\mathscr{E}(k)}{\tau(k)}, \tag{14.82}$$

which, because we demand that ε be constant, yields the famous law:

$$\mathscr{E}(k) = \mathscr{K}\varepsilon^{2/3}k^{-5/3}, \tag{14.83}$$

where $\mathscr{K}$ is a universal, hopefully order one, constant. This spectral form has been verified many times observationally, the first time using some very high Reynolds number oceanographic observations [19].

The scaling relationship [Eq. (14.83)], as well as some other useful scaling relationships, can be obtained in a slightly different, but essentially equivalent, way as follows. If we for the moment ignore viscosity, the equation of motion (14.1) is invariant under the following scaling transformation:

$$x \Rightarrow x\lambda \qquad v \Rightarrow v\lambda^r \qquad t \Rightarrow t\lambda^{1-r}, \tag{14.84}$$

where r is an arbitrary scaling exponent. So far there is no physics. Now make the following physical assumptions: First we make the locality hypothesis, namely that the energy flux through a wavenumber k depends only on local quantities [namely, the wavenumber itself and the energy $\mathscr{E}(k)$ or velocity $v(k)$]. Second, the flux of energy from large to small scales is assumed finite and constant. Third we assume that the scale invariance (14.84) holds, on a time-average, in the intermediate scales between the forcing scales and dissipation scales. This is likely to be strictly valid only in the limit of infinite

Reynolds number, but for finite Reynolds number it is made plausible by the locality hypothesis. [It is important to note that the infinite Reynolds number limit *is* a limit, and is different from simply neglecting the viscous term in Eq. (14.1), which gives the so-called Euler equations. This is because, as we shall see, this term contributes even in the zero-viscosity limit.] The time average in practice need be no longer than a few longest eddy turnover times, and depending on how local the energy transfer actually is we do not need an infinite Reynolds number for the scaling to be valid in the inertial range.

Dimensional analysis then tells us that the energy flux scales as

$$\varepsilon \sim \frac{v^3}{l} \sim \lambda^{3r-1}, \tag{14.85}$$

from which the assumed constancy of ε gives $r = 1/3$. This has a number of interesting consequences.

The velocity scales as $v \sim \varepsilon^{1/3} k^{-1/3}$. The velocity gradient scales as $\nabla v \sim \varepsilon^{1/3} k^{2/3}$, as does the vorticity $\omega = \nabla \times \mathbf{v}$. These quantities thus blow up (i.e., become infinite) at very small scales, but this is in fact avoided by a viscous cut-off.

We can now recover Eq. (14.83) easily, because dimensionally

$$\mathcal{E} \sim v^2 k^{-1} \sim \varepsilon^{2/3} k^{-2/3} k^{-1} \sim \varepsilon^{2/3} k^{-5/3},$$

which is Eq. (14.83).

The structure functions S_m of order m, which are the average of the m'th power of the velocity difference over distances $l \sim 1/k$, scale as $(\delta v_l)^m \sim \varepsilon^{m/3} l^{m/3} \sim \varepsilon^{m/3} k^{-m/3}$. In particular the second-order structure function, which is the fourier transform of the energy spectra, scales as $S_2 \sim \varepsilon^{2/3} k^{-2/3}$.

The viscous effects effects become important at a range given by equating the viscous and inertial terms in Eq. (14.1); that is

$$\nu k^2 v \sim k v^2,$$

which yields

$$k_\nu \sim \left(\frac{\varepsilon}{\nu^3}\right)^{1/4}. \tag{14.86}$$

The scale $l_\nu \sim k_\nu^{-1}$ is called the *Kolmogorov scale*. In the limit of viscosity tending to zero, l_ν tends to zero, but the energy dissipation, perhaps amazingly, does not. The energy dissipation is given by

$$\dot{E} = \int \nu \mathbf{v} \cdot \nabla^2 \mathbf{v} \, d\mathbf{x}. \tag{14.87}$$

Because the length at which dissipation acts is the Kolmogorov scale, this expression scales as (for a box of unit volume)

$$\dot{E} \sim \nu k_\nu^2 v^2 \sim \nu \frac{\varepsilon^{2/3}}{k_\nu^{2/3}} k^2 \sim \varepsilon, \tag{14.88}$$

with $k = k_\nu$. Hence, energy dissipation apparently does not depend on the viscosity at all! This result is actually quite consistent with the whole picture. Energy is input at some large scales, and the magnitude of the stirring largely determines the energy input and cascade rate. The scale at which viscous effects become important is determined by the value of the molecular viscosity by Eq. (14.86). If viscosity tends to zero, this scale becomes smaller and smaller in such a way as to preserve the constancy of the energy dissipation.

Finally, the time scales as $t \sim \lambda^{2/3}$, implying that for smaller scales the "eddy-turnover time," on which structures at that scale deform, becomes smaller and smaller.

Two-Dimensional Turbulence

In two dimensions the situation is complicated by another quadratic invariant, the enstrophy. Taking the curl of Eq. (14.1) to give a vorticity equation, and restricting attention to two-dimensional flows, yields the vorticity equation:

$$\frac{\partial \zeta}{\partial t} + \mathbf{u} \cdot \nabla \zeta = \nu \nabla^2 \zeta, \tag{14.89}$$

where $\mathbf{u} = u\mathbf{i} + v\mathbf{j}$ and $\zeta = \mathbf{k} \cdot \text{curl } \mathbf{u}$. It is easily verified that when $\nu = 0$, Eq. (14.89) conserves not only the energy but also the enstrophy $Z = \int \frac{1}{2}\zeta^2 \, d\mathbf{x} = \int k^2 \mathcal{E}(k) dk$.

We now ask, how does the distribution of energy and enstrophy change in a turbulent flow? The problem is analogous to that of rearranging mass on a lever while still preserving the moment of inertia, with energy playing the role of mass, enstrophy that of moment of inertia, and wave number the distance from the fulcrum. Any rearrangement of mass such that its distribution also becomes wider must be such that the center of mass moves toward the fulcrum. Thus, energy would move to *smaller* wave numbers and enstrophy to larger. Consistent with this, it is easy to show that energy dissipation goes to zero as Reynolds number rises. The total dissipation of energy is, from Eq. (14.89),

$$\frac{dE}{dt} = -\nu \int \zeta^2 \, d\mathbf{x}. \tag{14.90}$$

Because vorticity itself is bounded from above [again using Eq. (14.89)] we see that energy dissipation goes to zero as viscosity goes to zero, and hence also in the infinite Reynolds number (but finite energy) limit. Thus, unlike the three dimensional case, there is no mechanism for the dissipation of energy at small scales in high Reynolds number two-dimensional turbulence. On the other hand, we do expect enstrophy to be dissipated at large wave numbers.

These arguments lead one to propose the following scenario in two-dimensional turbulence. Energy and enstrophy are input at some scale L_I and energy is transferred to larger scales (toward the fulcrum), and enstrophy is cascaded to small scales where ultimately it is dissipated. In the enstrophy

inertial range the enstrophy cascade rate η is assumed constant. Using the dimensionally correct scaling

$$\eta \sim \frac{k^3 \mathscr{E}(k)}{\tau(k)} \tag{14.91}$$

yields the prediction

$$\mathscr{E}(k) = \mathscr{K}' \eta^{2/3} k^{-3}, \tag{14.92}$$

where $\mathscr{K}'$ is also, it is supposed, a universal, order one, constant. It is of course also quite possible to obtain Eq. (14.92) from scaling arguments identical to those following Eq. (14.84). The scaling transformation (14.84) still holds, but now instead of (14.85) we assume that the enstrophy flux is constant with wave number. Dimensionally we have

$$\eta \sim \frac{v^3}{l^3} \sim \lambda^{3r-3}, \tag{14.93}$$

which gives $\lambda = 1$. The exponent n determining the slope of the inertial range is given, as before, by $n = -(2r+1)$ yielding the -3 spectra of Eq. (14.92). Thus, the velocity now scales as $v \sim \eta^{1/3} k^{-1}$, and the time scales with distance as $t \sim l/v \sim \eta^{-1/3}$. Thus, it is length-scale invariant. The appropriate Kolmogorov scale is given by equating the inertial and viscous term in Eq. (14.1) or (14.89), which gives, analogously to (14.85)

$$k_\nu \sim \left(\frac{\eta^{1/3}}{\nu}\right)^{1/2}. \tag{14.94}$$

The energy dissipation is easily calculated to go to zero as $\nu \to 0$. The enstrophy dissipation, analogously to Eq. (14.88), goes to a finite limit given by

$$\begin{aligned} \dot{Z} &= \frac{d}{dt} \int \frac{1}{2} \zeta^2 \, dx = \nu \int \zeta \nabla^2 \zeta \\ &\sim \nu k_\nu^4 v^2 \sim \eta. \end{aligned} \tag{14.95}$$

So far so good. However, things in two dimensions are, unfortunately, not quite as simple as they appear. First, note that timescale given by Eq. (14.81) is apparently independent of scale. If the spectra were any steeper, then turnover times would actually increase with wave number. In fact the estimate Eq. (14.81) of an eddy turnover time is actually rather poor for the steep spectra found in two dimensional turbulence, and a useful refinement is:

$$\tau = \left\{ \int_{k_0}^{k} (p^2 \mathscr{E}(p)) \, dp \right\}^{-1/2}, \tag{14.96}$$

where k_0 is a lower wavenumber cut-off, recognizing the straining effects of all velocity scales larger than the scale of interest. Using this in Eq. (14.90)

yields the log-corrected range

$$\mathscr{E}(k) = \mathscr{K}'\eta^{2/3}(\log(k/k_0))^{-1/3}k^{-3}. \tag{14.97}$$

This is likely to be observationally indistinguishable from the uncorrected range. (Generally speaking, we can safely leave out logarithmic corrections in final results, if not always in intermediate calculations. We will subsequently neglect them.)

However, this has not fixed the underlying problem with the two-dimensional phenomenology, which is as follows. The inertial range predictions are based on the assumption of locality, in spectral space, of energy and enstrophy transfers. Now, a useful measure of this locality is given by the straining at a particular wavenumber, say k, from other wavenumbers. The total strain $T(k)$ at k is given by

$$T(k) = \left\{\int_0^k \mathscr{E}(p)p^3 d\log p\right\}^{1/2}. \tag{14.98}$$

The contributions to the integrand from each octave are given by

$$\mathscr{E}(p)p^3\Delta \log p. \tag{14.99}$$

In three dimensions, use of the $-5/3$ spectra indicates that the contributions from each octave below k increase with wave number, being a maximum close to k, implying locality and a posteriori being consistent with the locality hypothesis. However, in two dimensions each octave makes the same contribution. The strain, and possibly the enstrophy transfer, are hardly local after all! This very heuristic result implies that the two-dimensional phenomenology is on the verge of not being self-consistent, and suggests that the -3 spectral slope is the shallowest limit that is likely to be actually achieved in nature or in any particular computer simulation, rather than a very robust result. Why? Well, suppose the detailed dynamics attempt in some way to produce a shallower slope; using Eq. (14.99) the strain is then local and the shallow slope is forbidden by the Kolmogorovian scaling results. However, if the dynamics organizes itself into structures with a steeper slope (say k^{-4}), the strain is quite nonlocal. The fundamental assumption of Kolmogorov scaling is not satisfied, and there is no inconsistency. In fact numerical simulations do reveal a slope steeper than k^{-3}, often dominated by isolated vortices. However, the dynamical processes leading to their formation, and their precise relationship with the enstrophy cascade, are not at this time fully understood.

There is one other aspect of the phenomenology that has been sometimes thought to be a problem, but in fact is not. This is that in the limit of zero viscosity, Eq. (14.95) implies that enstrophy dissipation remains constant, whereas it has been shown rigorously that the inviscid equations—Eq. (14.89) with the right-hand side set to zero—have no singularities and enstrophy dissipation remains zero. This is not in fact a contradiction, first because we are concerned with the zero viscosity *limit* in Eq. (14.95). Even if we were to sud-

denly 'turn off' the viscosity in an infinitely high resolution simulation of Eq. (14.89), then the enstrophy inertial range (assuming it exists) would slowly spread to larger and larger wave numbers. During this period of adjustment the fluid indeed has zero enstrophy dissipation. It takes the fluid an infinite time to come to equilibrium with an infinitely long inertial range. Only then is the enstrophy dissipation nonzero, which is not an inconsistency with the rigorous results.

14.4.2 Predictability of Strong Turbulence

One of the central properties of turbulence is its unpredictability due to nonlinear interactions. Some authors will draw a distinction between "sensitive dependence on initial conditions" and "unpredictability." The former's meaning is unambiguous, and it is normally applied to deterministic systems. The latter is sometimes applied only to indeterminism arising out of stochasticity, when the equations of motion are not known. However, in this chapter we take them to be synonymous, and use the latter (because it is but one word) to mean unpredictability arising from chaos. Actually, the difference between chaos and stochasticity lies not so much in the underlying dynamics, but in our knowledge of them. Whereas chaos is essentially but a word for deterministic "randomness," stochasticity describes randomness arising from incomplete knowledge of the system, as for example in Brownian motion. Thus, in most cases the difference between stochasticity and chaos may be thought of as merely a difference in our knowledge of the dynamics. For example, most computers have "random number generators" built in, and these are often used in the simulation of stochastic systems. However, the algorithm producing the random numbers is completely deterministic, and if we regard that algorithm as part of the system, we have chaos, not stochasticity.

The modern ideas of nonlinear dynamics and chaos have not, interestingly enough, had at this time much impact on theories of, or ideas of how to cope with, strong turbulence. Even prior to the classical paper of Lorenz in 1963 and later Ruelle and Takens in 1971, it was believed that turbulence was truly unpredictable [9], notwithstanding the picture of Landau of turbulence as a large collection of periodic, and presumably predictable, motions. The unpredictability was thought to arise from the utter complexity of the flow. The reasons for the loss of predictability were probably only properly understood when it was realized that even systems with a small number of degrees of freedom could be unpredictable. Assuming that the dynamical systems arguments applicable to weak turbulence apply to strong turbulence, and hence that a turbulent fluid *is* in fact unpredictable, then just using the scaling laws we can heuristically obtain estimates of the predictability time for a turbulent fluid [20].

The physical space fields $\zeta(\mathbf{x})$ may be expressed as an infinite Fourier sum or integral, for example $\zeta = \sum \hat{\zeta}_{\mathbf{k}} \exp(i\mathbf{x}\cdot\mathbf{k})$ or $\zeta = \int \hat{\zeta}_{\mathbf{k}} \exp(i\mathbf{x}\cdot\mathbf{k})\, dk$. The former is appropriate in a bounded domain (where the wave numbers are

quantized), the latter in an infinite domain. We are usually concerned with a finite domain, but will nevertheless often replace sums by integrals where it will simplify things. In two dimensions (for simplicity) the inviscid vorticity equation may be written in spectral form

$$\frac{\partial \zeta_k}{\partial t} + \sum a_{kpq}\zeta_p\zeta_q = -\nu k^2 \zeta_k, \tag{14.100}$$

where a_{kpq} are geometrical coupling coefficients which arise when Eq. (14.89) is Fourier transformed. The hats over transformed quantities have been dropped. At any given instant the equation of motion may be linearized about its current state, and the subsequent motion would then be described by an equation, valid for short times, of the form:

$$\frac{\partial \zeta'_k}{\partial t} + A_{kq}\zeta'_q = 0, \tag{14.101}$$

and the eigenvalues of the matrix A_{kq} (whose explicit form does not concern us here) determine the short-term growth of errors in the system. Because the system is chaotic, A_{kq} has positive (growing) eigenvalues. If spectral interaction in the inertial range are sufficiently local, it becomes meaningful to inquire as to the growth of errors at any particular scale k, for then the matrix A_{kq} is dominated by terms close to its diagonal. In particular, the rate of error growth at any particular scale is then given by the size of the appropriate coefficient of A_{kq}, which is ku_k where u_k is just a typical velocity at scale k. This of course is just the inverse of the eddy turnover time (14.81). After a time τ_k, errors will have grown sufficiently that a linear approximation is no longer valid; at that scale errors will saturate but at the same time will begin to contaminate the "next larger" (in a logarithmic sense) scale, and so on. Thus, errors initially confined to a scale k at $t = 0$ will contaminate the scale $2k$ after a time τ_k. The total time taken for errors to contaminate all scales from k' to the largest scale k_0 is then given by, treating the wavenumber spectrum as continuous,

$$\begin{aligned} T &= \int_{k_0}^{k'} \frac{d(\ln k)}{\tau_k} \\ &= \int_{k_0}^{k'} \frac{d(\ln k)}{\sqrt{k^3 E(k)}}. \end{aligned} \tag{14.102}$$

If the energy spectrum is a power law of the form $E = C'k^{-n}$ this becomes

$$T = [C'k^{(n-3)/2}]_{k_0}^{k'} \frac{2}{(n-3)}. \tag{14.103}$$

As $k' \to \infty$ the estimate diverges for $n > 3$, but converges if $n < 3$.

What does this mean? First, we should point out that these arguments are at best heuristic, and do not account for the more esoteric phenomena, such as intermittency and coherent structures, believed by many to be important in

strong turbulence. Nevertheless, taking them at face value they imply that two-dimensional turbulence is indefinitely predictable; if we can confine the initial error to smaller and smaller scales of motion, the payoff is that the "predictability time" (the time taken for errors to propagate to all scales of motion) can be made longer and longer, indeed infinite. This is consistent with what has been rigorously proven about the two-dimensional Navier–Stokes equations, with or without viscosity; namely, that they exhibit "global regularity," meaning they stay analytic for all time provided the initial conditions are sufficiently smooth (Rose and Sulem [4]). This does *not* mean that two-dimensional flow is in practice necessarily predictable. Two-dimensional turbulence is almost certainly chaotic, has positive Lyapunov exponents, and an arbitrarily small amount of noise will render a flow truly unpredictable sometime in the future. It is just that we can put off that time indefinitely if we know the initial conditions well enough, and can reduce the amount of external noise sufficiently.

In three dimensions, on the other hand, things are more worrisome. The predictability time estimate from Eq. (14.103) converges as $k' \to \infty$ so that even if we push our initial error out to smaller and smaller scales, the predictability time does not keep on increasing. The time it takes for errors initially confined to small scales to spread to the largest scales is simply a few *large* eddy turnover times (because the eddy turnover times of the small scales are so small). This is an indicator that something is badly wrong, either with our methodology or with the Euler equations; because the system is classical, we do not expect such finite time catastrophes. If one were able to prove global regularity for the three-dimensional Euler equations then we would know our analysis was wrong, but such a proof is lacking, and may not exist. So it is still an open question as to whether the equations are well posed or not. If the Euler equations were ill posed, it would mean that they are an incorrect description of zero-viscosity turbulent flow, which would perhaps not be so terrible anyway as no classical flow is inviscid, and we would be saved from having to throw away the Navier–Stokes equations by viscosity. No matter how small viscosity, if not zero, then at some small wave number the local Reynolds number will be small and viscous effects will start to dominate over inertial effects. Beyond the dissipation wave number, it is possible to show that the energy spectrum gets steeper, and as soon as the asymptotic spectra is steeper than -3 we are again assured of indefinite predictability. If the Navier–Stokes equations were shown to have singularities, it would be a more serious matter.

So what about the weather? Well, in the lower part of the atmosphere (below 10 km, where the weather is) the large-scale flow behaves more like a two-dimensional fluid than a three-dimensional fluid. This is because of the twin effects of rotation and stratification, but we shall not go into that here. At scales smaller than about 100 km, the atmosphere starts to behave three-dimensionally. Now the current atmospheric observing system is such that over continents the atmosphere is fairly well observed down to scales of a

couple of hundred kilometers. If we knew the enstrophy cascade rate through the atmosphere we could evaluate the predictability time using the formulae derived above, but it is easier simply to do the sum manually, Fourier transforming in our heads, as it were. Suppose then we have no knowledge of the dynamical fields at scales smaller than 200 km. Aside from certain rather intense small-scale phenomena, the atmosphere is not especially energetic at these scales (hurricanes, for example, are rather larger as well as being intermittent) and we could estimate a typical velocity of about 1 m/s giving an eddy turnover time of about 2 days. So in 2 days motion at 400 km scales is unpredictable. The dynamics at these scales is a little more intense, say $U \sim 2$ m/s. Coincidentally (?), this also gives a 2-day eddy turnover time, so after 4 days motion at 800 km is unpredictable. Continuing the proccess, after about 12 days motion at 6000 km is completely unpredictable, and our weather forecasts are essentially useless. This is probably a little better than our experience suggests as to how good weather forecasts are in practice, but of course our models of the atmosphere are certainly not perfect. (Actually, I've fudged the numbers so they come out reasonable, having been rather cavalier about factors of 2, π, etc. More careful calculations, as well as computer simulations, do give similar results though.) In principle, we could make better forecasts if we could observe the atmosphere down to smaller scales of motion. Observing down to 100, 50, and 25 km would (if the atmosphere remained two dimensional) each add about a couple of days to our forecast times.

However, we can't go on forever, because at small scales of motion the atmosphere starts behaving three-dimensionally. As we have seen, because the energy spectrum for three-dimensional turbulence is shallow, the eddy turnover times decrease rapidly with scale and the predictability time is largely governed by the predictability time of the largest scale of motion. Thus, the *theoretical* limit to predictability is governed by the scale at which the atmosphere turns three dimensional, probably about 100 km. So we see that we can't increase the length of time we can make good weather forecasts for longer than about 2 weeks, no matter how good our models and no matter how good our observing system. This is the theoretical predictability limit of the atmosphere. The so-called butterfly effect has its origins in this argument: a butterfly flapping its wings over the Amazon is, so it goes, able to change the course of the weather a week or so later. How farfetched is this? Well, the affect of a lone butterfly are probably drowned both by viscous dissipation and more energetic eddies at larger scale. So although this argument may be an exaggeration, there is little doubt that small-scale phenomena will affect global weather some time later in an unpredictable manner.

One other point may be apposite. The predictability of a system is often characterized by its spectrum of Lyapunov exponents. In a turbulent system the largest Lyapunov exponent is likely be associated with the smallest scales of motion, and the error growth associated with this effectively saturates at small scales. The time scales of error growth affecting the larger scales, which

are the time scales of most interest, are determined by slower, larger-scale processes whether or not the cascade-like growth of error described above is correct. This means that the largest Lyapunov exponents probably have nothing whatever to do with the growth of error at the larger scales in a turbulent fluid.

14.4.3 Renormalizing the Diffusivity

To obtain a predictability time for the large scales of turbulence, we successively summed the effects of the smaller scales. I'd now like to briefly discuss one other application of this kind of approach, the idea now being to successively average over the smaller scales to produce an effective eddy diffusivity for the large scales. This is the same idea used in renormalization group techniques in condensed matter physics and discussed earlier with reference to transition problems, but the arguments given here will be simple and self-contained. Nevertheless, the discussion may be a little brief for those with no background in turbulence theory. Let us first discuss the problem.

A turbulent fluid may have many decades of scales of motion. Indeed, in the most-observed fluid of all (the earth's atmosphere) the forcing scales are several thousands of kilometers and the dissipation scales are perhaps order millimeters. Nevertheless, we cannot hope to explicitly describe all these scales of motion, even with future generations of computers. (If we attempted to do so by constructing a numerical model of the atmosphere with grid points every millimeter, it would take a time longer than the current age of the universe to advance just one time step, even with computers 10 times as fast as today's.) If we just use the value of the molecular viscosity in a model resolving only the large scales, energy will not be removed correctly, if at all. This means that in an equation such as (14.89) we must use a much larger viscosity, appropriate to these resolved scales, which represents the effects that subgridscale, or unresolved, motions have on those resolved. Because models of the large scales *can* be constructed and run on the computer, the problem of turbulence lies, in a nontrivial sense, in deriving an expression for such an "eddy viscosity."

As a step toward that goal, we will discuss a simpler problem, that of the eddy diffusivity of a passive tracer. Such a tracer (ϕ) obeys the equation

$$\frac{\partial \phi}{\partial t} + (\mathbf{u} \cdot \nabla)\phi = \kappa \nabla^2 \phi, \tag{14.104}$$

where κ is the molecular diffusivity, akin to the viscosity. The Peclet number, UL/κ is analogous to the Reynolds number and is a measure of the size of the inertial terms to the diffusive terms. Again, the problem arises as to what to do if our model does not reach the small scales at which the diffusivity is effective; we must derive an effective eddy diffusivity appropriate for high Peclet number regimes. The problem is, or at least should be, simpler than the eddy viscosity problem because Eq. (14.104) is a linear equation.

Just as there is a cascade of energy (in three dimensional turbulence) to the small scales there is a cascade of tracer variance, ϕ^2-stuff, from large scales to small. Scaling arguments similarly give rise to inertial range predictions for the spectrum of tracer variance. These are:

$$\Phi(k) = C\chi k^{-5/3}\varepsilon^{-1/3} \tag{14.105}$$

in three dimensions and

$$\Phi(k) = C'\chi k^{-1}\eta^{-1/3} \tag{14.106}$$

in two dimensions, where C and C' are undetermined, dimensionaless, constants and χ is the rate of cascade of tracer variance, $\Phi(k)$.

At sufficiently small scales the Peclet number becomes of order unity and dissipation of ϕ^2-stuff occurs. If the diffusivity is sufficiently large, diffusion occurs before (i.e., at larger wave numbers) than dissipation of energy by viscosity. Because Eq. (14.36) is linear, it turns out that it is possible (after a great deal of algebra [21]) to derive an expression for the eddy diffusivity, in a certain *low Peclet number limit*. The expression is

$$\mathscr{D}(k) = \frac{2}{3}\int_k^\infty \frac{\mathscr{E}(p)}{\kappa p^2}\,dp. \tag{14.107}$$

This is a sensible and unsurprising result, because it merely says that the eddy diffusivity is determined by the combined motion of small eddies from a size $1/k$ and smaller. The result is of no immediate help, because it is valid only in a low Peclet number limit.

Note that Eq. (14.107) contains the actual molecular diffusivity in the denominator. Now, suppose that Eq. (14.107), or an expression very similar to it, is accurate at some wavenumber k, in the dissipation regime, and we wish to obtain an expression for the eddy diffusivity at some slightly larger scale, or smaller wave number $k - \Delta k$. Then at $k - \Delta k$ the correct expression for the eddy diffusivity will be the value at k plus a small contribution from the wavenumber interval between k and $k - \Delta k$. But in this interval, the diffusivity appearing in the denominator should not only be the molecular diffusivity, but should include the eddy diffusivity appropriate at that wavenumber. That is:

$$D(k - \Delta k) = D(k) + \frac{2\mathscr{E}(k)}{3(\kappa + D(k))}\frac{\Delta k}{k^2}. \tag{14.108}$$

Thus, given the result valid for low Peclet number, we are able by successive applications of Eq. (14.108) to bootstrap ourselves to a result valid in a low wave number, high Peclet number regime (see [22]). From Eq. (14.108) we obtain the differential equation

$$\frac{\partial D}{\partial k} = -\frac{2}{3(D + \kappa)}\frac{\mathscr{E}(k)}{k^2}, \tag{14.109}$$

which integrates, with the boundary condition of $D(\infty) = 0$, to give

$$D(k) = -\kappa + \left[k^2 + \frac{4}{3}\int_k^\infty \frac{\mathscr{E}(p)}{p^2}\,dp\right]^{1/2}. \tag{14.110}$$

In the low Peclet number limit, the expression is strongly dependent on the molecular value. In the high Peclet number limit Eq. (14.110) simply reduces to

$$D(k) = \left[\frac{4}{3}\int_k^\infty \frac{\mathscr{E}(p)}{p^2}\,dp\right]^{1/2} \tag{14.111}$$

and there is no explicit dependence on the molecular diffusivity. We have apparently succeeded, then, in obtaining a "renormalized" value of the diffusivity, which would be appropriate to use in calculations that do not explicitly resolve the diffusive subrange.

It is possible to use Eq. (14.111) to make testable predictions about the values of $\mathscr{K}$ and $\mathscr{K}_t$ appearing in the inertial range expressions (14.83) and (14.105), and (14.92) and (14.106), for energy and passive tracer variance in three and two dimensions, respectively. To do this first evaluate Eq. (14.111) using Eq. (14.83) or (14.92) to give

$$D_3(k) = \left(\frac{\mathscr{K}}{2}\right)^{1/2} \varepsilon^{1/3} k^{-4/3} \tag{14.112}$$

in three dimensions and

$$D_2(k) = \left(\frac{\mathscr{K}'}{3}\right)^{1/2} \eta^{1/3} k^{-2} \tag{14.113}$$

in two. Now, the dissipation of tracer variance (ϕ^2-stuff) in reality is given by

$$\chi = \kappa \int_0^\infty p^2 \Phi(p)\,dp. \tag{14.114}$$

Similarly, it is also equal to

$$\chi = D(k) \int_0^k p^2 \Phi(p)\,dp, \tag{14.115}$$

where the upper limit may now lie in the inertial range. For the three-dimensional case, substituting Eq. (14.105) for $\Phi(p)$ and Eq. (14.112) for $D(k)$, and performing the integration, gives a relationship between $\mathscr{K}$ and C, namely

$$C = \frac{4}{3}\left(\frac{2}{\mathscr{K}}\right)^{1/2}. \tag{14.116}$$

Experimentally, C and $\mathscr{K}$ are both approximately 1.5, which is consistent with the prediction.

In two dimensions, a similar calculation yields

$$C' = \left(\frac{12}{\mathscr{K}'}\right)^{1/2}. \tag{14.117}$$

There is currently no experimental confirmation or falsification of this prediction. However, because the Kolmogorov scaling itself in two dimensions remains unconfirmed, this may be moot.

It is tempting, but unjustified on any a priori basis, to suppose that in two-dimensions the above ideas apply not only to a passive tracer but also to vorticity—for note that Eq. (14.89) is the same form as Eq. (14.104). Then from Eq. (14.116) we obtain a prediction for the value of the Kolmogorov constant by setting $C' = \mathscr{K}'$, to give $\mathscr{K}' = 12^{1/3}$. We emphasize that this last step is very speculative, although there are a couple of indicators that it may not be completely nonsensical [23]. First, numerical simulations do indicate that at the small scales of two-dimensional turbulence the vorticity field is passively advected by the large field. Second, a subsequent but independent full renormalization group treatment gave, perhaps remarkably, precisely the same numerical number for $\mathscr{K}'$. It may be that such a treatment is implicitly treating the vorticity as passive, although it is difficult to disentangle the assumptions from the very elaborate calculations. In any case, as this stage our reach has now far exceeded our grasp (but then what's a heaven for?) and we should now sum up.

14.5 Remarks

In this chapter we first discussed some basic notions of linear instability and nonlinear equilibration. Then, temporarily leaving the Navier–Stokes equations behind, we discussed various sequences to do with the transition to chaos. Much progress has undeniably been made in understanding the transition problem using tools from "nonlinear science" or dynamical systems theory. However, for the physicist these would be little more than mental gymnastics were it not for the fact that a number of the sequences have actually been observed in experiment. The experimental verification is important because at the time of writing there is something of a gap between the scaling theories and rigorous mathematical hydrodynamics. Ideally, one would like to be able to do the following: take the Navier–Stokes equations for some fairly generic geometry (e.g., three-dimensional convection in a box of arbitrary aspect ratio, or a rotating cylinder) and show that a series of rational approximations for some particular range values of control parameter (say Rayleigh number or Reynolds number) leads to a low-dimensional map or system of ordinary differential equations for which the transition to instability and then chaos is well understood. Although in some circumstances this goal can be approached, in general it is a very difficult proposition—it is even difficult to rigorously obtain the appropriate Landau equation for a given instability,

and this is a simpler task than elucidating the full transition sequence. In the absence of this it is very difficult to predict ahead of time what particular route a given flow will take, or even to say with confidence that the transition to turbulence is understood. Numerical simulations and algebraic manipulation languages, such as Maple, will undoubtedly help, as will using any symmetry in the geometry.

The astute reader will also have noticed that there was no section entitled "From Chaos to Turbulence." This lamentable lack is not solely due to laziness or ignorance on the part of the author, although both may be applicable. It is because little is quantitatively understood about the phenomenon. It is certain that turbulence is chaotic, although it is not certain how the transition from low-dimensional chaos to higher-dimensional turbulence occurs, whether it is in any sense universal, even whether it is a sensible question, and so on.

Bypassing this difficult topic, we then turned to strong turbulence. Although scaling arguments prove useful in understanding the basic phenomenology, further progress at a fundamental level has here too been slow. However, a lot of useful practical information, for example the predictability limits of the atmosphere, can be estimated using no more than these arguments. We then discussed a rather more recondite topic, that of renormalizing the eddy diffusivity in a turbulent flow using a successive averaging approach. Such arguments have proved successful in a number of problems involving many scales of motion, and their application to turbulence is attractive because they apparently afford a means of beginning with an expression or idea valid in a rather restrictive domain and bootstrapping to a regime of greater validity. Nevertheless, more sophisticated application of renormalization group theory has been a little controversial and there currently is probably no a priori reason to prefer them over the more established renormalized perturbation theories.

It is a truism to say that fluid mechanics in general is difficult because it is nonlinear. Turbulence in particular is made even more difficult by the fact that it involves many degrees of freedom, or put another way, its dimensionality is large. The impact of ideas in nonlinear dynamics, which have typically dealt only with systems of low dimensionality, on strong turbulence is yet to be seen. It may not be too important to understand the detailed structure of the strange attractor in turbulence (presuming that the attractor is strange); because the flow is so complex, any interesting properties manifest themselves before the attractor has been fully explored. However, it is probably true to say that the generic lack of predictability of fluid motion, as dictated and explained by the presence of strange attractors in turbulence, actually *underscores the necessity* for a statistical theory rather than a deterministic theory of turbulence. Whether the texture of what is traditionally meant by nonlinear dynamics (chaos, strange attractors, Lyapunov numbers, etc.) will play a direct role in turbulence is unclear; rather the ideas may provide theoretical foundation for statistical assumptions. In any case, the field (as it has

been since Horace Lamb, in the 1920s, expressed more faith in the Almighty being able to explain quantum electrodynamics than turbulence) is ripe for progress.

References

[1] A.S. Monin and A.M. Yaglom, *Statistical Fluid Mechanics: Mechanics of Turbulence*, Vols. I and II. (MIT, Cambridge, 1971).

[2] P. Drazin and W.H. Reid, *Hydrodynamic Stability* (Cambridge University, Cambridge, 1981); *Hydrodynamic Instabilities and the Transition to Turbulence*, 2nd ed., edited by H.L. Swinney and J.P Gollub (Springer-Verlag, New York, 1985).

[3] B. Hu, Phys. Rep. **91**, 233 (1982); L.D. Landau and E.M. Lifshitz, *Fluid Mechanics*, 2nd ed. (Pergamon, Oxford, 1987).

[4] J. Miles, Adv. Appl. Mech. **24**, 189 (1984); J-P. Eckmann, Rev. Mod. Phys. **53**, 643 (1981); H. Rose and P.-L. Sulem, J. Phys. **39**, 441 (1978).

[5] R. Kraichnan, J. Fluid Mech. **5**, 497 (1959).

[6] F.M. Ludlam, *Clouds and Storms: the behavior and effect of water in the atmosphere*. (Pennsylvania State University, Philadelphia, 1980).

[7] C. Bender and S. Orszag, *Advanced Mathematical Methods for Scientists and Engineers* (McGraw-Hill, New York, 1978).

[8] T. Stuart, J. Fluid Mech **9**, 353 (1960); J. Watson, J. Fluid Mech. **9**, 370 (1960); J. Pedlosky, J. Atmos. Sci. **27**, 15 (1970).

[9] P.D. Thompson, Tellus **9**, 275 (1957); Ye.A. Novikov, On the predictability of synoptic processes. Izv. An. SSSR. Ser. Geophys **11**, (1959).

[10] D. Ruelle and F. Takens, Comm. Math. Phys. **20**, 167 (1971).

[11] M.J. Feigenbaum, J. Stat. Phys. **19**, 25 (1978); M.J. Feigenbaum, J. Stat. Phys. **21**, 669 (1979).

[12] Y. Pomeau and P. Manneville, Comm. Math. Phys. **74**, 189 (1980); P. Manneville and Y. Pomeau, Physica D **1**, 219 (1980).

[13] J. Collet and J.-P. Eckmann, *Iterated Maps on the Interval as Dynamical Systems* (Birkhauser, Boston, 1980).

[14] J.P. Gollub, S.V. Benson, and J.A. Steinman, Ann. NY Acad. Sci. **357**, 22 (1980); M. Giglio, S. Musazzi, and U. Perini, Phys. Rev. Lett. **47**, 243 (1981); A. Libchaber, C. Laroche, and S. Fauve, J. Phys. Lett. **43**, 211 (1982).

[15] D.R. Moore, J. Toomre, E. Knobloch, and N.O. Weiss, Nature **303**, 663 (1983).

[16] J. Gollub and S.V. Benson, J. Fluid Mech. **100**, 449 (1980).

[17] A. Libchaber and J. Maurer, J. Phys. Colloq. **41**, 51 (1980).

[18] A.N. Kolmogorov, Doklady AN SSSR **30**, 299 (1941).

[19] H.L. Grant, R.W. Stewart, and A. Moilliet, J. Fluid Mech. **12**, 241 (1962).

[20] C.E. Leith and R.H. Kraichnan, J. Atmos. Sci., **29**, 1041 (1972); G.K. Vallis, Q.J. Roy. Meteor. Soc. **111**, 1039 (1985); G.K. Vallis, in *Nonlinear Phenomena in the Atmospheric and Oceanic Sciences*, edited by G. Carnevale and R. Pierrehumbert (Springer-Verlag, New York, 1992).

[21] G.K. Batchelor, I.D. Howells, and A.A. Townsend, J. Fluid Mech. **5**, 134 (1959); I.D. Howells, J. Fluid Mech. **9**, 104 (1960).

[22] H.K. Moffatt, J. Fluid Mech. **106**, 27 (1981).

[23] M.E. Maltrud and G.K. Vallis, Phys. Fluids A **5**, 1760 (1993); P. Olla, Int. J. Mod. Phys. B **8**, 581 (1994).